TRABAJO FIN DE MÁSTER

Máster en Nanociencia y Nanotecnología Molecular

Chitosan-based Molecularly Imprinted Polymers for the detection of compounds of interest in the food industry

Autor:

Antonio Joaquín Martín Pinillos

Tutores:

María Luz Rodríguez Méndez

Coral Salvo Comino

Valladolid, 2024

Index

Summary

The use of sensors in the food industry is essential to control and guarantee the organoleptic properties of their products. For this purpose, the preparation of sensors to easily measure the different compounds present in food has generated an enormous interest.

Molecularly imprinted polymers (MIPs) can act as electrochemical sensors purposely designed to have specific recognition cavities. This cavities are shaped by the use of a definite template molecule present during the formation of the sensor. Once the molecularly imprinted polymer is formed, the template molecule is eluted leaving behind the specific cavities. The presence of this cavities will later be crucial in the selective detection of a specific concentration range of solutions containing the template molecule.

In this work, MIP sensors have been developed using the electrodeposition of a biopolymer, chitosan, via cyclic voltammetry in a glassy carbon electrode. The parameters of this electrodeposition have been optimized in this work, modifying mainly the use of cross-linking agent as well as the pH of the chitosan solution. For the optimization, the response of the sensor towards catechol using cyclic voltammetry was evaluated in comparison to the use of a non-imprinted polymer (NIP), prepared under the same conditions but in the absence of template molecule.

Also, the effect of introducing metallic nanoparticles has been tested in order to see how they affect the intensity of response of the sensors. In this case gold (AuNPs) and silver (AgNPs) nanoparticles have been used.

Once optimized, MIP sensors have been developed to detect organic acids present in the food industry, successfully obtaining sensors for the detection of lactic, malic and tartaric acid.

All of the prepared MIP sensors gave a limit of detection in the order of 10^{-5}M or lower in the detection of the compound they were designed for. The addition of nanoparticles, even though it gave positive results, was discarded due to the balance between the higher cost of operation and the improvement of the results

Keywords

Food industry, electrochemical sensors, MIP, cyclic voltammetry, chitosan, catechol, AuNPs, AgNPs, lactic acid, malic acid, tartaric acid.

Introduction

2.1. Industry 4.0.

Industry is a segment of the economy focused on producing material goods, heavily reliant on mechanization and automation. The term "industrial revolution" denotes significant changes in industrial processes brought about by new technologies. From the onset of industrialization, technological advances have led to major paradigm shifts: the first industrial revolution introduced mechanization, the second saw the intensive use of electrical energy, and the third was characterized by widespread digitalization.[1,2,3]

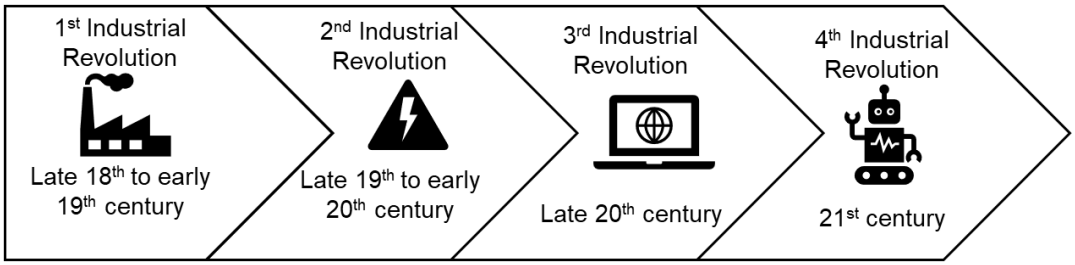

Figure 1. Timeline of the Industrial revolutions

Building on advanced digitalization within factories, combining Internet technologies with forward-looking technologies in the realm of “smart” objects (machines and products) seems poised to trigger another fundamental paradigm shift in industrial production. Future production visions include modular and efficient manufacturing systems where products manage their own manufacturing processes.[4]

The concept of the fourth industrial revolution was first mentioned in Germany at the “Hannover Fair” in 2011 by Klaus Schwab and was presented to the public at the 2015 World Economic Forum. Industry 4.0 represents an era of cyber-physical systems, encompassing AI, robotics, machine learning (ML), nanotechnology, biotechnology, quantum computing, blockchain, the Internet of Things (IoT), and 3D printing, among others.[5]

A significant technology push is evident in industrial practice, influencing daily routines. Several approaches highlight this technology push:[4]

1. **Increased Mechanization and Automation**: The use of technical aids to support physical work will expand, with automatic solutions taking over diverse operations, including operational, dispositive, and analytical tasks. Examples include autonomous manufacturing cells that independently control and optimize various manufacturing steps.

2. **Miniaturization**: There is a trend towards miniaturization, where devices with significant computing power are now much smaller. This enables new applications, particularly in production and logistics.
3. **Smart Factory**: Manufacturing will be fully equipped with sensors, actuators, and autonomous systems. "Smart Factories," driven by digital models of products and factories (digital factories) and various ubiquitous computing technologies, will emerge, featuring autonomous control.
4. **Corporate Social Responsibility**: Sustainability and resource efficiency are increasingly central to industrial manufacturing processes, forming essential conditions for successful products.

Technological advancements span numerous areas, notably computing, nanotechnology, biotechnology, materials science, and energy. Ongoing Industry 4.0 research primarily focuses on software and data algorithms. In this automated and interconnected environment, nanotechnology plays a crucial role. Nanotechnology enhances sensors by increasing their sensitivity and robustness, thus minimizing data acquisition errors and expanding potential applications in previously unsuitable environments.[6,7]

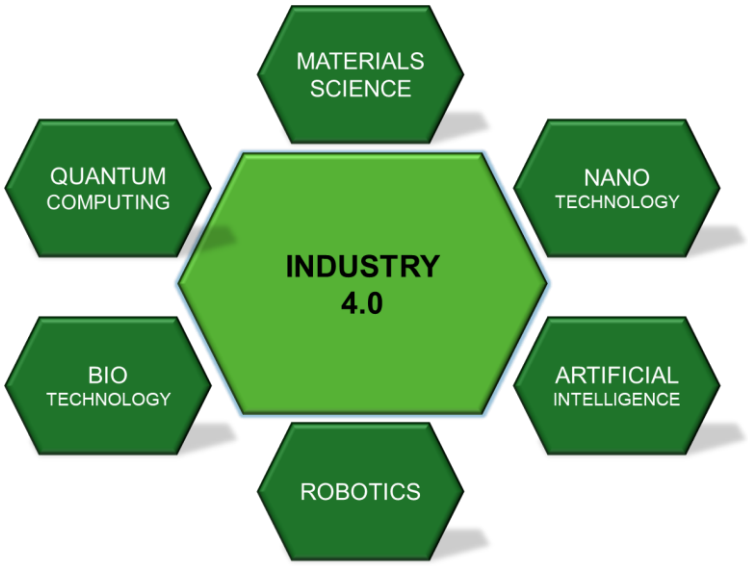

Figure 2. Industry 4.0 components

Quantum computing also benefits significantly from nanotechnology, with semiconductor nanomaterials enhancing processing speed and data transmission security—key features for Industry 4.0. Additionally, nanotechnology facilitates the creation of an "Internet of Nano Things" (IoNT), a network at the nano level that holds great potential for telecommunications and medical fields.[8]

Artificial intelligence, machine learning, and big data platforms, underpinned by nanotechnology, are foundational to the fourth industrial revolution. Vast amounts of raw data collected through interconnected devices are processed and analyzed to improve

understanding and efficiency. Machine learning, in particular, excels in modeling future behavior, sentiment analysis[9], and inventory management, streamlining production chains.

Drone and robotics technology is another dimension where nanotechnology and computing converge. These technologies have diverse applications in maintenance, inspections, transportation, and data collection. Advanced drones and robots, integrated with IoT, enhance automation and precision in industries, reducing costs and errors. This integration, termed the "Internet of Robotics and Nano Things," increases manufacturing flexibility and dexterity compared to traditional robotics.[10]

Materials used in Industry 4.0 must meet the high demands that the applications require them, with advanced composites and smart materials being essential for new applications compatible with emerging technologies like 3D printing and CNC milling. Innovations in nanotechnology have led to materials like graphene, which offer significant advancements in device performance and manufacturing processes. These materials support sustainability and efficiency, aligning with circular economy principles and expanding the potential of existing manufacturing technologies.[11,12]

Figure 3. Graphene, an example of material developed and used in Industry 4.0.

2.2. Nanoscience and Nanotechnology

The prefix 'nano' originates from the Greek word meaning 'dwarf' or something very small, and it denotes one thousand millionth of a meter (10^{-9} m).

Nanoscience is a field of science dedicated to the study of materials that are smaller than 100 nanometres at least in one dimension. Nanoscience involves the use of techniques and knowledge of chemistry, physics and biology. **Nanotechnology** is the development of devices, products or processes based on nanocomponents using the application of nanoscience.[13]

Both nanoscience and nanotechnology are relatively new fields that are attracting a lot of interest these days since new properties arise when the size decreases to the nanometre scale.

Richard Feynman (1918-1988) is considered as one of the fathers of this field, being his lecture *"There's Plenty of Room at the Bottom"* which he presented in 1959 important to settle the basis of what nanotechnology is. Nowadays his lecture is used as an important inspiration in this field.[14]

Is important to mention also **Norio Taniguchi** (1912-1999), the first researcher to describe the concept of nanotechnology. In 1974, Taniguchi defined the term nanotechnology as: "nanotechnology mainly consists of the processing of separation, consolidation, and deformation of materials by one atom or one molecule".[15]

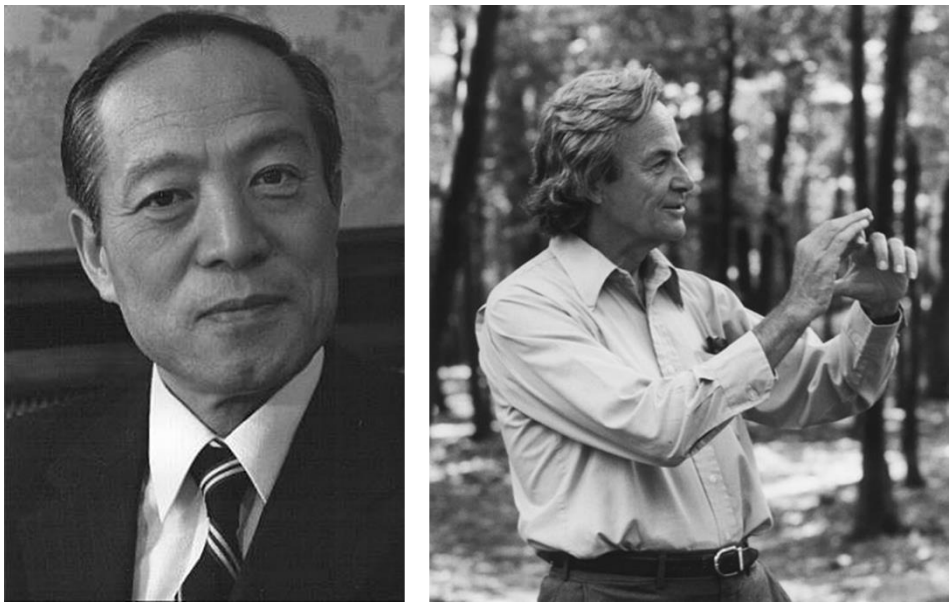

Figure 4. Picture of Norio Taniguchi (left) and Richard Feynman (right).

After Feynman discovered this new field of research, which caught the interest of many scientists, two approaches were developed to describe the different possibilities for

synthesizing nanostructures. These manufacturing approaches fall into two categories: top-down and bottom-up, which vary in terms of quality, speed, and cost.

The **top-down approach** involves breaking down bulk material to obtain nano-sized particles. This can be achieved using advanced techniques such as precision engineering and lithography, which have been developed and optimized by industry over recent decades.

In contrast, the **bottom-up approach** involves constructing nanostructures atom-by-atom or molecule-by-molecule using physical and chemical methods at the nanoscale, through controlled manipulation and self-assembly of atoms and molecules. Chemical synthesis produces raw materials that can be used directly in products in their bulk disordered form or as building blocks for more advanced ordered materials. Self-assembly, a bottom-up technique, involves atoms or molecules organizing themselves into ordered nanostructures through chemical-physical interactions.[16]

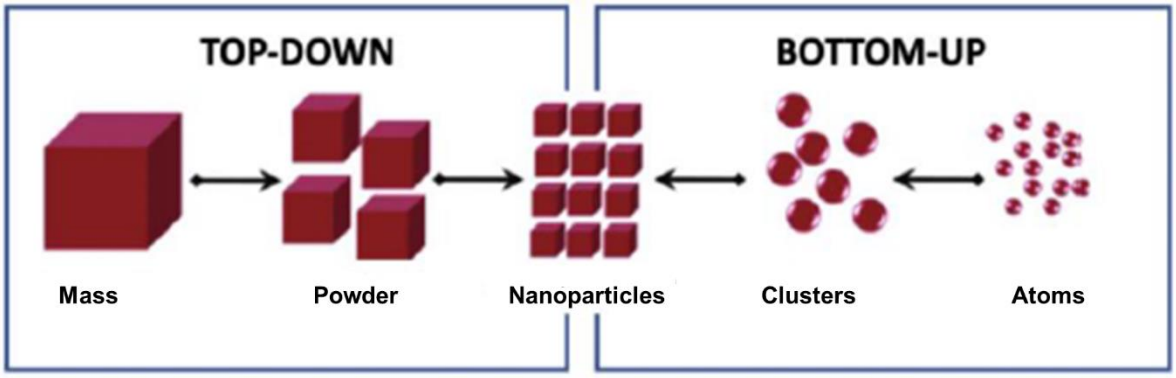

Figure 5. Representation of Top-Down and Bottom-Up approaches.

Nanotechnologies contribute to nearly every field of science, including physics, materials science, chemistry, biology, computer science, and engineering. The progress of nanoscience and nanotechnology has expanded in various directions, allowing for observation at scales from micro to nano and even smaller using different microscopes in physics, from bulk matter to carbon dots in chemistry, from room-sized computers to slim laptops in computer science, and from the behaviour of the cell's nucleus to single biomolecules in biological science.

In just a few decades, nanotechnology and nanoscience have become fundamentally important for industrial **applications** and medical devices, such as diagnostic biosensors, drug delivery systems, and imaging probes. For example, in the food industry, nanomaterials have significantly increased production, packaging, shelf life, and the bioavailability of nutrients. Zinc oxide nanostructures, for instance, display antimicrobial activity against food-borne bacteria, and various nanomaterials are now used for diagnostic purposes as food sensors to detect food quality and safety.[17]

The area of **nanostructured materials**, or nanomaterials, is particularly fascinating and continues to attract interest due to its immense potential as the materials of the future. Achieving this goal requires large quantities of materials with complex nanostructures and ongoing development and research in this area. Nanomaterials are being used to build new generations of solar cells, hydrogen fuel cells, and novel hydrogen storage systems capable of delivering clean energy to countries still dependent on traditional, non-renewable fuels. Additionally, nanostructured sensors are notable for their unique features, including chemical, physical, and surface effects due to their increased surface-area-to-volume ratio. These sensors are highly efficient, working at an atomic scale to provide better selectivity and sensitivity, very low energy consumption, fast response times, and rapid recovery.[18]

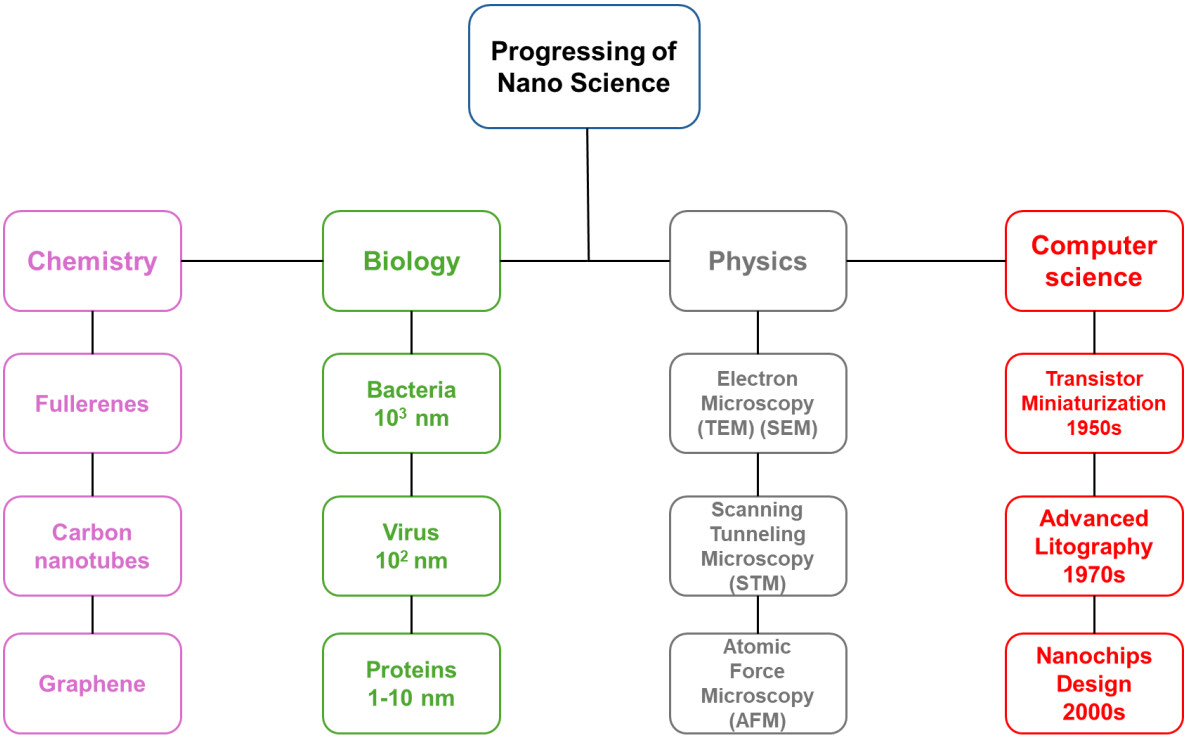

Figure 6. Progress in nanoscience and nanotechnology in different fields of science.

2.3. Chemical sensors

Chemical sensors are devices that convert a chemical parameter into an electrical signal. This chemical parameter can be concentration, activity, partial pressure of particles such as atoms, molecules, ions or biologically relevant compounds to be detected in the gas, liquid or solid phase.[19]

Chemical sensors can be classified based on various properties used for particle detection. All chemical sensors may be distributed depending on the transducing system in six principal groups, among others: **Electrochemical sensors** are potentiometric (ion selective electrodes ISE, ion selective field-effect transistors ISFET) and voltammetric, electrolytic gas sensors, and semiconductor gas sensors; **Optical sensors** (optodes) exploit optical spectra for functioning; **Mass-sensitive sensors** include devices based on the use of surface acoustic waves (SAW-sensors); **Thermometric sensors**, measure the heat effects resulting from specific chemical reactions or adsorption involving the analyte; **Electrical sensors**, this devices rely on measurements where no electrochemical processes occur, the signal results from changes in electrical properties due to interaction with the analyte; and **Magnetic sensors**, which utilize changes in the paramagnetic properties. All of the sensors specified may be applied either separately or within combinations (analyzer of an "electronic tongue" type), in which the sensors may take various shapes and sizes.[20,21]

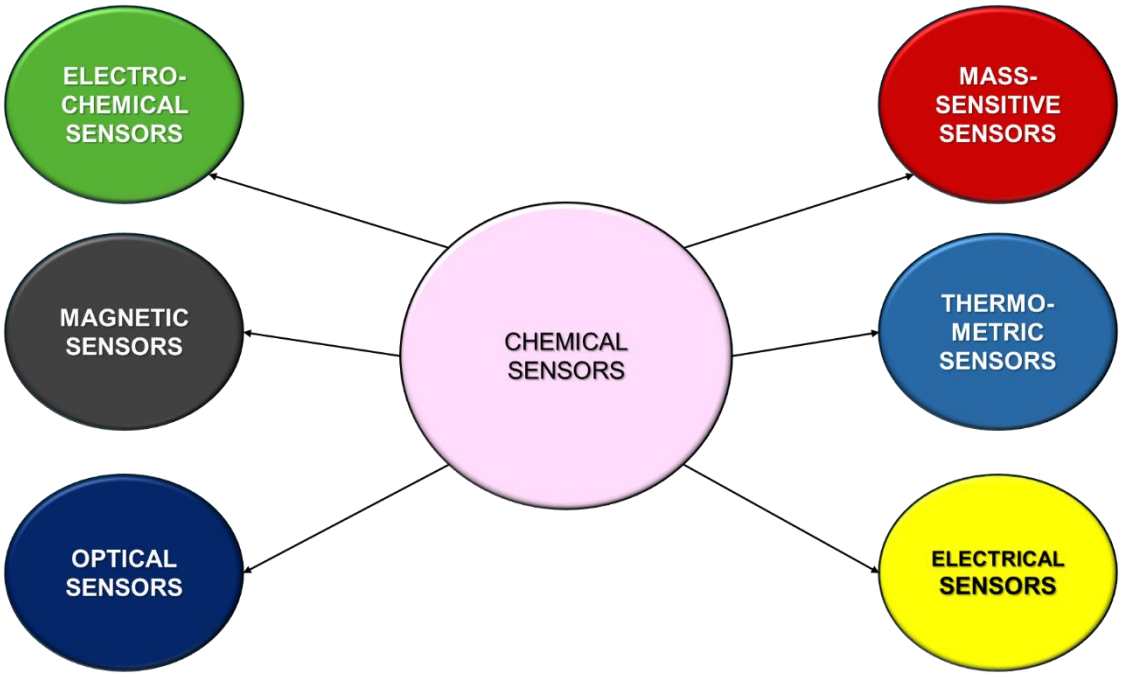

Figure 7. Classification of chemical sensors.

The development of sensors is a multidisciplinary endeavor involving knowledge from diverse fields such as chemistry, physics, electrical engineering, electronic engineering, and computer science. It is noteworthy that designing different types of chemical sensors

(inorganic, organic, bioorganic) necessitates employing distinct technologies. A critical aspect in designing chemical sensors is mastering **interface phenomena**. Interfaces and surfaces can exhibit reversible interactions between sensors and particles, or they may remain inert without undergoing chemical reactions.

As previously mentioned, a specific type of chemical sensors are electrochemical sensors. **Electrochemical sensors** are sensors based on the relation of concentrations, partial pressures or activities of chemical species with measured potential differences and electrical currents. These type of sensors are easy to calibrate and don't require a very complex equipment. Electrochemical sensors can sense and measure concentrations and activities of ions and neutral species in liquid solutions, solids and gases.

2.3.2. Voltammetric sensors

There are multiple types of **electrochemical sensors**: **Conductimetric sensors**, that detect changes in conductivity; **Potentiometric sensors**, devices that measure the potential difference between working electrode and a reference electrode at zero current; **Amperometric sensors**, whose signals depend on the charge transfer rate at the electrode surface; **Impedance sensors**, where measurements focus on changes in the charge transfer resistance; and **Voltammetric sensors**, that measure current intensity variation over an applied potential interval. We are going to focus on these last type of electrochemical sensors.

Voltammetry is considered as a highly sensitive electrochemical method based on the measurement of the current intensity due to electron transfer processes when a bias voltage is applied. It gives the possibility of varying potential range, scan rates and the nature of the working electrode in order to measure the oxidation/reduction response of the analytes.[22]

Cyclic voltammetry is the name given to the technique that applies a potential from an initial potential E_i to a final potential E_f with the particularity that, once reached E_f, the direction of the potential scan is reversed, stopping normally at the initial potential E_i. The process of going back to the initial potential is called **cycle** and can be performed multiple times.[23]

This technique produces plots called **cyclic voltammograms**, in this type of plots both oxidation and reduction peaks can be observed. If E_f is bigger than E_i, then the oxidation peak occurs during the forward part of the voltammogram while the reduction peak will take place during the reverse part. If E_f is smaller than E_i then the opposite will happen, with the reduction peak appearing during the forward part, and the oxidation peak showing up during the reverse part.

The classical experimental configuration to record cyclic voltammograms is based on an electrochemical cell with three electrodes, counter or auxiliary electrode (C), reference electrode (R), and working electrode (W), all of them immersed in solution and connected to a potentiostat. The potentiostat controls the potential difference between the reference and working electrode.[24]

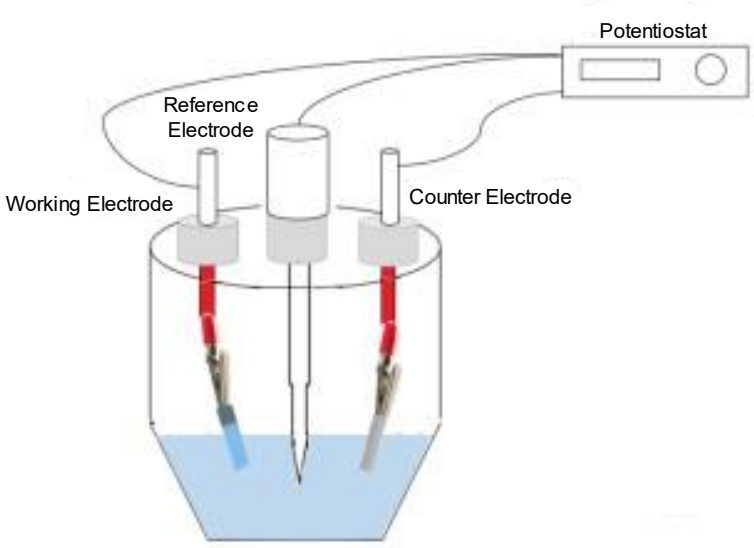

Figure 8. Cell for cyclic voltammetric experiments with three-electrode configuration.

The electrodes commonly used for cyclic voltammetric experiments are:

- **Reference electrode**: typical ones are aqueous Ag/AgCl or calomel half cells, as they can be prepared with ease in the laboratory or obtained commercially.

- **Counter electrode**: a high surface area and non-reactive electrode, normally platinum.

- **Working electrode**: well defined area electrodes normally with inlaid disc geometry (Pt, Au, graphite, glassy carbon, etc.). Also, different geometries may be employed (cylinder, band, arrays, or grid electrodes) beneficially in the corresponding situation.

Voltammetric sensors can be defined as devices that can detect and measure a specific chemical property, such as concentration, activity or partial pressure, by applying voltammetric techniques. They have multiple reported applications in various fields, including food analysis[25,26], environmental monitoring[27,28] and clinical diagnostics[29,30] among others.

The selectivity of a sensor is established by its capability to detect concentrations of particular ions amidst other ions in a solution. However, **chemical sensors** often exhibit **partial selectivity**, with their measurements influenced by interfering ions. Overcoming this limitation involves exploring new membrane materials, with nanomaterials showing promise in this regard.

The electrode also plays an important role in voltammetric sensors, influencing their sensitivity, selectivity, and overall performance. The material composition (e.g., carbon-based, metal, composite), surface area and morphology (e.g., nanostructured, porous), and surface modifications critically affect the electrochemical properties and detection

capabilities. Electrode size and geometry, along with proper conditioning and pre-treatment, further impact mass transport, background currents, and stability. The incorporation of electrocatalytic materials can enhance reaction kinetics and lower detection limits, while nanomaterials, such as nanoparticles and nanowires, can significantly increase the surface area and improve electron transfer rates.

2.4. Molecularly Imprinted Polymers

One of the main tools that nanotechnology gives us to improve the selectivity of our sensors are molecularly imprinted polymers.

Molecularly Imprinted Polymers (MIPs) are polymers with the imprint of a particular molecule called template molecule. Molecular imprinting is used to create cavities in polymeric matrixes where the cavities adopt the shape of the **template molecule**. They are synthetic analogues of natural biological antibody-antigen systems. Using a "lock and key" mechanism, they selectively bind to the molecule for which they were templated during production. MIPs offer the specificity and selectivity of biological receptors, along with the added benefits of durability in various environmental conditions and low cost. Unlike biological systems, where the target must match an existing antibody or an antibody must be specially produced, MIPs can be created for nearly any target molecule. Additionally, MIPs are generally less expensive compared to natural antibodies.[31]

There are various production methods available, but the general method has the next **four steps**: first, monomers organise around the molecule; secondly, monomers are polymerized; thirdly, the template molecule is removed leaving behind a cavity with his shape; and finally, the MIP is put under presence of the sample containing the target. The second step can be altered with the use of a polymer instead of a monomer, the polymer also organises around the molecule, but in the second step this polymer is electrodeposited enclosing the template molecule.

There are two similar approaches, one of them involves the formation of covalent bonds between the polymer and the template molecule and the other approach involves the use of non-covalent interactions, like ionic and hydrogen bonding. In both cases these interactions occur in solution previous to the polymerization step.[32]

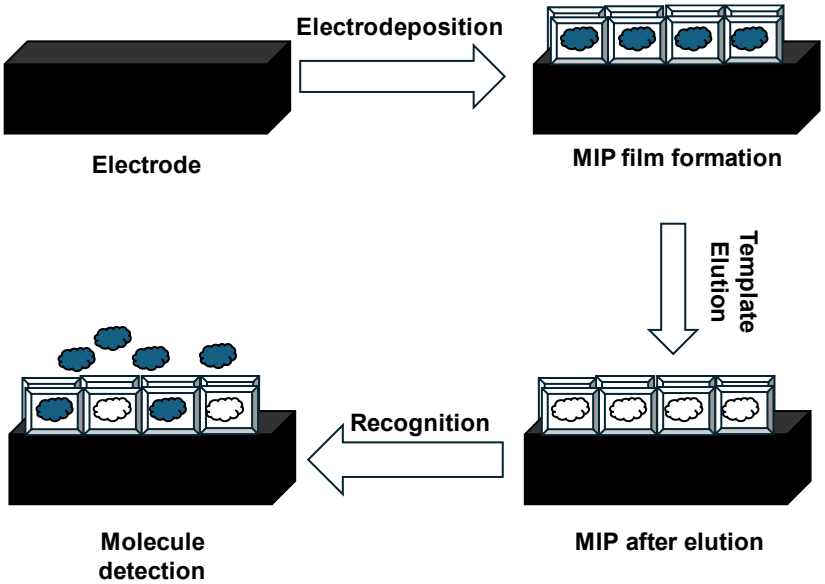

Figure 9. MIP obtention steps.

Choosing the right **polymer** is crucial for creating highly specific cavities tailored to be specific to the template molecule. Common functional monomers include carboxylic acids (acrylic acid, methacrylic acid, vinylbenzoic acid), sulfonic acids (2-acrylamido-2-methylpropane sulfonic acid), and heteroaromatic bases (vinylpyridine, vinylimidazole).

The method of synthesizing MIPs typically involves a cross-linking component to create more rigid and uniform binding sites. **Crosslinking** is essential in MIP synthesis, as the choice and proportion of the crosslinking agent relative to the functional monomer significantly affect the polymer matrix's morphology and the selectivity of the cavities post-template extraction.[33] Crosslinking allows for:

- **Precise control** over template imprinting.
- **Enhanced interaction** complementarity with the target molecule.
- **Improved mechanical stability** of the polymer and imprints.
- **Formation of a robust matrix** that withstands high temperatures, pressures, and is inert to acids and bases.

Common cross-linking agents include ethylene glycol dimethacrylate (EGDMA) and trimethylolpropane trimethacrylate (TRIM).

Combining **MIPs** with a **transduction** system results in a device useful for detecting a variety of chemicals. A possible measurement method for MIP recognition polymers in sensors involve electrical techniques, which require electrode production. A electrocatalytic component is typically included by adding a conductive "reporting" layer above the electrodes or by creating a composite MIP with materials like carbon nanotubes, metallic nanoparticles, or conductive copolymers.

Electrochemical measurements for MIP-based sensors often include conductimetry, potentiometry, amperometry, **voltammetry**, and impedimetry. These techniques are mainly used with liquid samples and employ three electrodes: the MIP on the working electrode, paired with counter and reference electrodes in a cell. Their measurements correlate with the physical and chemical properties of the MIP-template interaction, and the choice of technique depends on the target molecule's electrochemical properties.[33]

However, developing MIP-based materials for sensors faces **challenges** due to nonspecific binding to the templated material. The polymer's inherent adsorptive properties lead to unavoidable weak interactions with the target molecule, and nonhomogeneous binding sites result in a range of rebinding constants, complicating the intended use. Using MIPs as sensors is further complicated by the need to extract the target molecule from the produced polymer. In some applications, any unextracted target can interfere with rebinding detection.[30]

2.5. Chitosan-based molecularly imprinted polymers

Chitosan (CS) is derived from chitin through a deacetylation process. It is a family of linear polysaccharides composed of D-glucosamine (DD molar fraction) and N-acetylglucosamine (fraction 1-DD). Chitosan acts as a copolymer featuring three reactive functional groups: a **primary amino group**, and primary and **secondary hydroxyl groups** (one primary amine group at C2 and two hydroxyl groups at C3 and C6 per repeat unit).[34]

Chitosan is a highly basic polysaccharide with cationic properties in acidic environments. It is a hydrophilic biopolymer and a highly polar molecule due to the numerous hydroxyl and amine groups in its glucosamine units. Each glucosamine unit in chitosan contains one NH_2 group and two OH groups, making these groups highly reactive and crucial to the polymer's properties.

The robust **functionality of chitosan** allows for extensive chemical modification. The amino groups provide a specific binding platform with external groups, which is a vital feature for biofabrication. Meanwhile, the hydroxyl groups add flexibility to the material and play a role in altering its biological and physical properties.[35]

Chitosan is unique as the only commercially available water-soluble cationic biopolymer. It dissolves in dilute acidic solutions at pH levels under 6.5 but remains insoluble in neutral and alkaline aqueous solutions.[36]

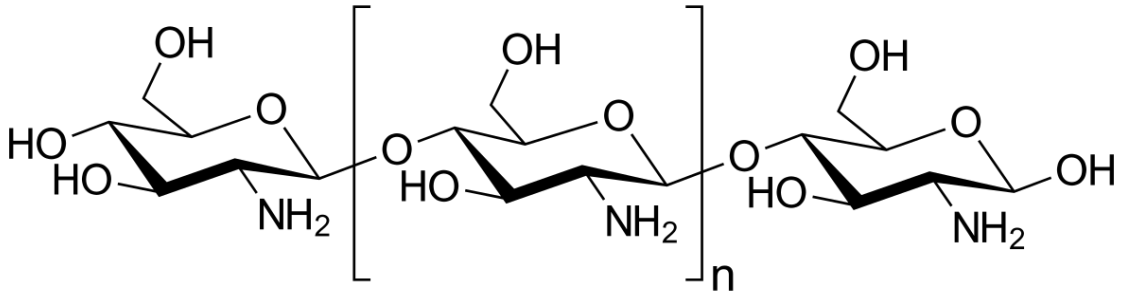

Figure 10. Chitosan structure.

The **classical monomers** used for MIP preparation are typically **insoluble** in aqueous solutions, which can be problematic for certain template molecules. Chitosan, a naturally abundant **biosourced polymer**, offers a solution. It presents easily modifiable functional groups, is biodegradable, and supports circular economy principles—unlike traditional monomers. These advantages make chitosan a compelling choice for preparing MIP sensors. Chemical crosslinking enhances the stability, compatibility, and mechanical properties of chitosan. Various **crosslinking agents**, such as **glutaraldehyde** and glyoxal, are commonly used with chitosan.[37]

Several types of sensors have been developed using **MIPs**, including electrochemical, colorimetric, and fluorescent sensors. **Electrochemical sensors** are particularly prevalent due to their simplicity, sensitivity, ease of implementation, and generally low measurement costs.

However, the electrochemical performance of electrodeposited chitosan films on working electrodes is limited by poor electrical conductivity. This is due to the high crystallinity of chitosan, which impedes the redox process.[38] To address this issue, **incorporating nanomaterials** with electroactive properties into the development of molecularly imprinted chitosan-based electrochemical sensors could be highly beneficial. Nanomaterials enhance electron transfer between the electrode surface and the solution, thereby improving the sensitivity of chitosan-based sensing materials.

Nanomaterials such as gold nanoparticles, **silver nanoparticles**, carbon nanocomposites, carbon nanotubes, graphene, and multiwalled carbon nanotubes can be used to modify electrodes due to their excellent electrocatalytic activity.[39,40]

2.6. Applications

Electrochemical sensors incorporating **molecularly imprinted chitosan** have demonstrated **excellent performance**. These sensors have shown a strong linear response to various targets, achieving low detection limits and exhibiting good selectivity, reproducibility, stability, and reusability.

Numerous successful instances of developing electrochemical sensors based on chitosan-MIPs for diverse types of template molecules have been reported:

With **metabolites** like dopamine, L-dopa, and urea as template molecules, whose significance spans multiple fields. **Dopamine** (DA) is a crucial catecholamine and neurotransmitter, essential for diagnosing conditions like schizophrenia and Parkinson's disease, necessitating its rapid and accurate measurement.[41] **Levodopa (L-Dopa)**, which addresses dopamine deficiencies and is used in Parkinson's treatment, can be toxic in high concentrations, highlighting the need for precise analytical methods in pharmaceuticals and biological fluids.[42] **Urea**, essential in water quality assessment, soil productivity, NH_3 pollution monitoring, food safety, and clinical diagnostics, requires accurate measurement to maintain public health and environmental quality.[43]

Using **pesticides** as template molecules, trichlorphon and glyphosate are notable examples. **Glyphosate** (N-(phosphonomethyl) glycine) is a widely used herbicide known for its chemical stability and resistance to photochemical degradation. This persistence means glyphosate remains in soil, water, plants, and various habitats, raising significant toxicological and environmental concerns.[44]

With **medications** as template molecules, clenbuterol and epinephrine are key examples. **Clenbuterol** (CLB), which accumulates in animal liver, fur, and retina, can cause food poisoning symptoms like muscle tremors and tachycardia when present in human food. Despite being banned as a growth promoter, it is still used illegally, making its detection vital for food safety.[45] **Epinephrine** (EP), a critical catecholamine neurotransmitter, regulates essential processes such as blood pressure and immune response. Accurate measurement of EP in biological fluids and pharmaceuticals is crucial for monitoring health and ensuring effective medical treatment.[46]

With **phenolic compounds** as template molecules, key examples include bisphenol A, p-nitrophenol, catechol, and 2,4,6-tribromophenol. **Bisphenol A (BPA)**, used in producing polycarbonate plastics and epoxy resins, is noted for its estrogenic activity and role as an endocrine disruptor, necessitating rapid and effective detection methods.[47] **p-Nitrophenol (PNP)**, important in acetaminophen synthesis and pesticide manufacture, can cause

serious health issues, including liver damage and systemic poisoning, highlighting the need for careful monitoring.[48,49] **Catechol**, present in various foods and beverages, offers antioxidant benefits and is crucial for preserving the quality of wine by maintaining its organoleptic properties.[38] **2,4,6-Tribromophenol (TBP)**, used in brominated flame retardants and other products, is found in environmental sources like food packaging and seafood. Its potential toxicity underscores the importance of developing detection methods to protect health and the environment.[50]

All the applications shown before make chitosan-based MIP sensors **promising** for the **detection of compounds** that can be present in **food industry.**

The use of **chitosan based MIP** sensors to detect **organic acids present in food industry** is particularly interesting. Detecting organic acids in the food industry is essential for maintaining product quality, consistency, and safety. **Tartaric acid** is crucial in winemaking for stabilizing the wine. It plays a significant role in maintaining the wine's desired acidity, which balances flavours and enhances freshness, thus ensuring that the final product meets quality standards and consumer expectations.[51] **Lactic acid** is important in fermentation processes for products such as yogurt, cheese, and pickles, where it contributes to the development of desirable flavours and textures while acting as a preservative. Monitoring lactic acid levels helps control the fermentation process, ensuring proper acidity and preventing spoilage or contamination.[52] **Malic acid** is used in a variety of food products, including fruit juices, candies, and baked goods, to enhance flavours and regulate acidity. Its presence helps achieve the desired acidity and stability, improving the overall taste and durability of processed foods.[53]

Furthermore, the use of this type of chitosan-based MIP sensors for this purpose has never been reported, which makes it even more attractive.

Objectives

The investigation group UVaSens, in which this Master Thesis was carried out, has a large experience in the preparation of nanostructured sensors using multiple techniques such as Langmuir-Blodgett or the layer-by-layer techniques among others to ensure a perfect control of the film structure of the modified electrode, being one of the top groups in sensors and biosensors development. In this context, the finding for a novel approach of preparing selective sensors turned the attention to the molecularly imprinting technique, specifically using a biopolymer such as chitosan, with whom the group had previous experience.

The objective of this Master Thesis was then to develop a new line of research preparing and optimizing chitosan-based MIP sensors with high selectivity, avoiding the use of specific biological compounds like enzymes, to detect compounds of interest in the food industry such as phenols or organic acids.

Impact on the Sustainable Development Goals

The Sustainable Development Goals (SDG) are a call for action by all countries – poor, rich and middle-income – to promote prosperity while protecting the planet. They recognize that ending poverty must go hand-in-hand with strategies that build economic growth and address a range of social needs including education, health, social protection, and job opportunities, while tackling climate change and environmental protection.[54]

There are 17 Goals all of them interconnected and stablished by the United Nations, who also states that is important to achieve them all by 2030. The 17 Sustainable Development Goals are the following:

- Goal 1: No Poverty
- Goal 2: Zero Hunger
- Goal 3: Good Health and Well-Being
- Goal 4: Quality Education
- Goal 5: Gender Equality
- Goal 6: Clean Water and Sanitation
- Goal 7: Affordable and Clean Energy
- Goal 8: Decent Work and Economic Growth
- Goal 9: Industry, Innovation, and Infrastructure
- Goal 10: Reduced Inequalities
- Goal 11: Sustainable Cities and Communities
- Goal 12: Responsible Consumption and Production
- Goal 13: Climate Action
- Goal 14: Life Below Water
- Goal 15: Life on Land
- Goal 16: Peace, Justice and Strong Institutions
- Goal 17: Partnerships

The work here presented has mainly an impact in Goal 9, this goal seeks to build resilient infrastructure, promote sustainable industrialization and foster innovation.

In this case, the production of sensors helps to control the industrial processes with accuracy, helping in the optimization of the use of resources. Also, in this same context, this molecularly imprinted polymers sensors are based on chitosan, which is a polymer that can be obtained from the transformation of leftovers of crustaceans, this contributes also to encourage sustainable industrialization.

Also, this work has a lesser impact in Goal 2, which one of its objectives is to ensure sustainable food production systems. The developed sensors help to control the optimum quantity of organic acids present in several foods, and also helps to control the food safety, which is key to ensure the correct conditions of food helping to prevent diseases.

Results and discussion

4.1. Electrodeposition of MIP based on Chitosan. Optimization of the preparation conditions

The preparation of the chitosan-based MIP sensor takes place via electrodeposition. In this process, chitosan, a linear polysaccharide derived from chitin, is solved in acidic media via primary amine protonation. The cationic polymer can be electrodeposited by applying an appropriate voltage onto a conductive electrode in the presence of the template molecule. During the electrodeposition, the polymer organises itself around the template molecule. The electrodeposition can be carried out using different techniques such as chronoamperometry, chronopotentiometry or cyclic voltammetry. The electrodeposition is followed by an elution step where the template molecule is removed from the polymeric matrix. Finally, a crosslinking process is carried out using glutaraldehyde that is used to fix the polymeric structure.

The preparation of MIPs is a complex process where multiple parameters can be controlled, consequently affecting the results obtained from the analysis. Our group has large experience in the preparation of sensors using multiple techniques related to nanoscience such as Langmuir-Blodgett or the layer-by-layer techniques among others, but had little experience in MIP sensors, so this work was novel approach for this group and the development of MIPs started from the beginning. The electrochemical conditions of the electrodeposition, including the use of cyclic voltammetry as the deposition method, as well as the voltage and the scan rate applied in the electrodeposition were taken from bibliography.[33]

In this work, three different parameters have been optimized: the pH of the chitosan solution, the concentration of the template molecule and the time of exposure to glutaraldehyde to achieve an appropriate crosslinking.

The optimization of the preparation parameters has been carried out using **catechol** as the template molecule due to his **redox activity,** that facilitates the observation of changes in intensity or shifts in oxidation-reduction peaks. All the experiments have been carried out using cyclic voltammetry, applying a varying potential from 0V to 1.2V, for 5 scans with a scan rate of 0.1V/s, in the analysis of a 10^{-3}M catechol solution in 0.1M KCl.

The first parameter optimized was the cross-linking using **glutaraldehyde vapours.** This is the last step of the production of MIPs, but it is the first parameter that needs to be optimized in order to ensure that the imprint of the template molecule is maintained after removing it from the surface. The first experiments were dedicated to evaluate the benefits of using glutaraldehyde as crosslinker. For this purpose, MIPs were prepared in the presence of 0.1M catechol and exposed to a 25% volume glutaraldehyde solution. The

corresponding NIPs were also prepared using the same conditions but in the absence of catechol.

The electrochemical response, towards a 10^{-3}M catechol solution in 0.1M KCl, of MIPs and NIPs exposed to glutaraldehyde was compared with the response of the electrodes covered with non cross-linked MIPs and NIPs. In this initial step, the exposure time to glutaraldehyde was 20 minutes (Figure 11).

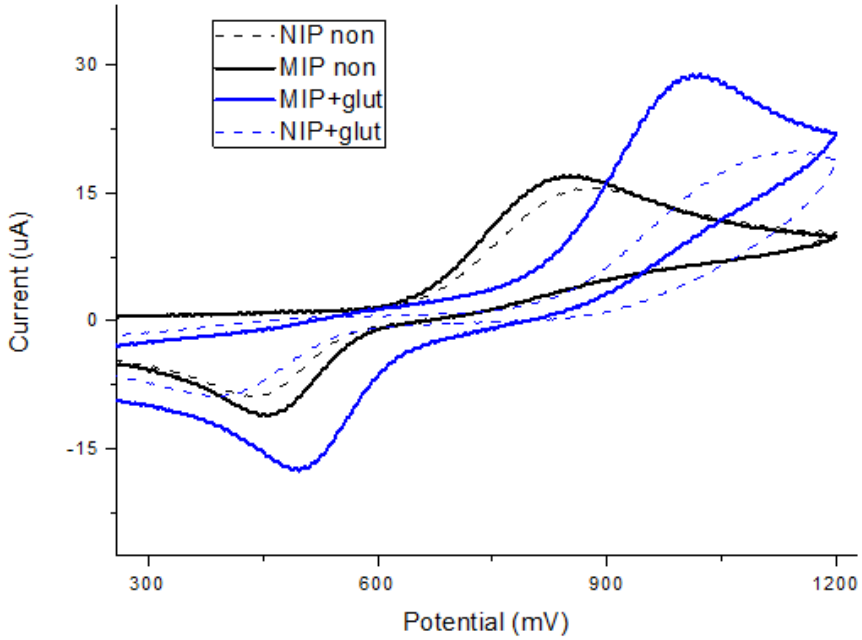

Figure 11. Voltammetric response of MIP and NIP towards catechol 10^{-3}M. Comparison between the exposition to glutaraldehyde vapours.

The voltammetric responses of MIPs and NIPs shows a quasi-reversible redox peak with E_a at 800 mV and E_c at 440 mV that correspond to the two electrons oxidation/reduction of catechol.[55] However, the response of the MIP is more intense than that of the NIP. This result indicates that catechol is oxidized/reduced at the surface of both electrodes, but in the case of MIP, the presence of holes with the appropriate shape increases the number of active sites producing an enhancement of the electrochemical signal.

In addition, it can be observed that the exposition of the electrode to glutaraldehyde vapours increases the intensity of the response of the MIP while the intensity of response of the NIP remains almost unaltered. Therefore, the exposition to glutaraldehyde vapours has a positive effect in maintaining the imprint of the molecule in the polymer.

Once determined that the electrode needs to be cross-linked the next step was to establish the correct time of exposition to glutaraldehyde vapors. This led to compare 20 minutes of exposure with larger exposure intervals of time such as 30 and 35 minutes:

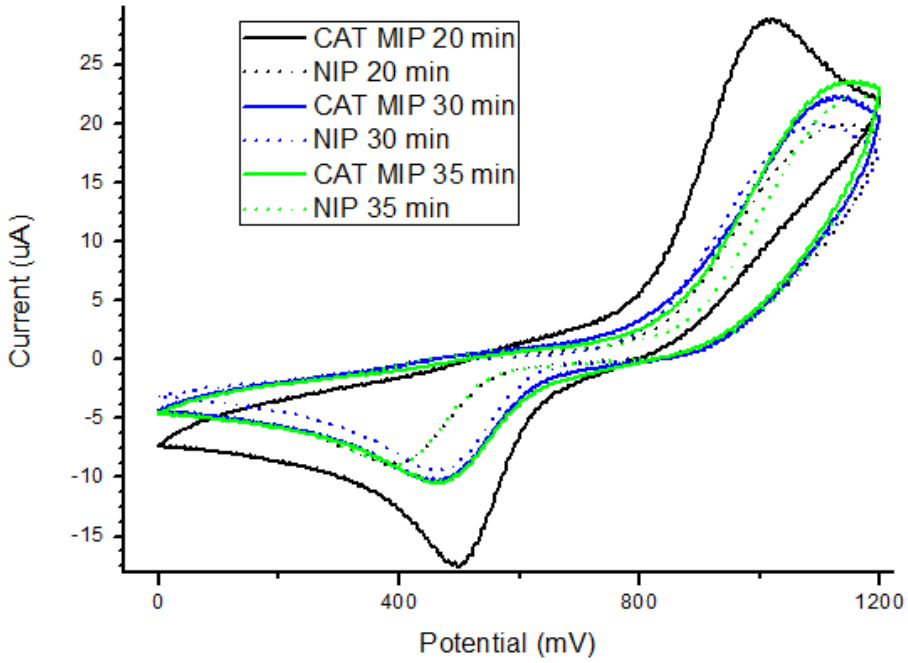

Figure 12. Exposition time to glutaraldehyde vapours comparison. Cyclic voltammogram of the analysis of a 10^{-3}M catechol solution. MIP and NIP were prepared using a 1.5mg/mL chitosan solution at pH 2.

As it can be seen in Figure 12, the best choice in terms of time of exposition to glutaraldehyde vapours is **20 minutes**, since this time of exposition gives clearly the most intense response of the MIP sensor. Ever since this point, the results shown were performed using a 20 minute time exposition to glutaraldehyde vapours.

After determining that the exposition to glutaraldehyde had to be done for 20 minutes, the next step was to evaluate the effect of the **pH of the chitosan (CS) solution**. In previous experiments, the pH of the CS solution was 2 (since chitosan needs to be solved in an acidic pH), so the pH was increased up to values of 3, 4 and 5. The pH adjustment was performed by the addition of NaOH.

Figure 13 shows that the highest intensity of response is obtained at pH 4, while the others values of pH show a lower intensity in comparison with pH 4. Therefore, from this point on, the chitosan solution will be adjusted to **pH 4**, so whenever the solution is mentioned it is important to have the consideration that the value of the pH will be 4.

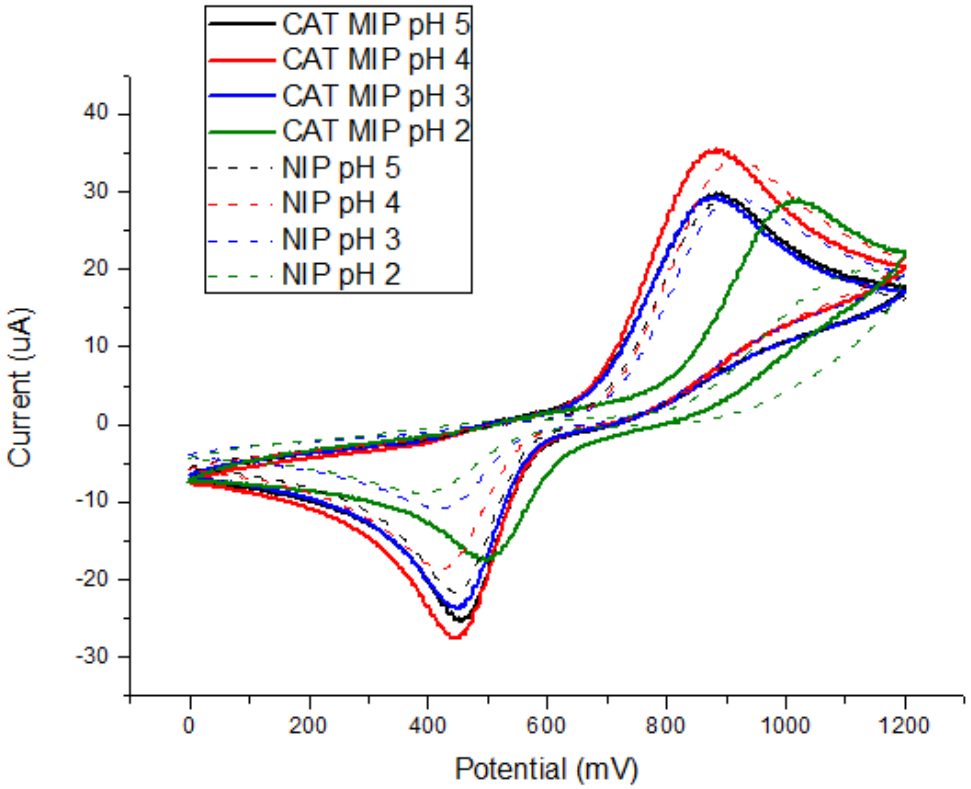

Figure 13. Analysis of the different responses to a 10^{-3}M catechol solution depending on the pH of the chitosan solution used to prepare the sensor.

In the preliminary studies shown before, a concentration of the template molecule of 0.1M of catechol was used to obtain the MIP. But the question was, to gain knowledge in the effect of the concentration of the template molecule.

The next parameter optimised was the **concentration of the template molecule, catechol in this case**.

Figure 14 shows a comparison between the employment of 0.1M of catechol and the employment of 0.01M catechol in the chitosan solution used to electrodeposit the polymer and thus the formation of the molecularly imprinted polymer. As it can be seen, there are almost negligible differences in the intensity of response of both MIPs, but the response of the MIP with 0.1M concentration of catechol is slightly more intense. Therefore, a 0.1M concentration is the chosen concentration and it is the one employed for the rest of MIPs, with the exception of the case of lactic acid which will be discussed later.

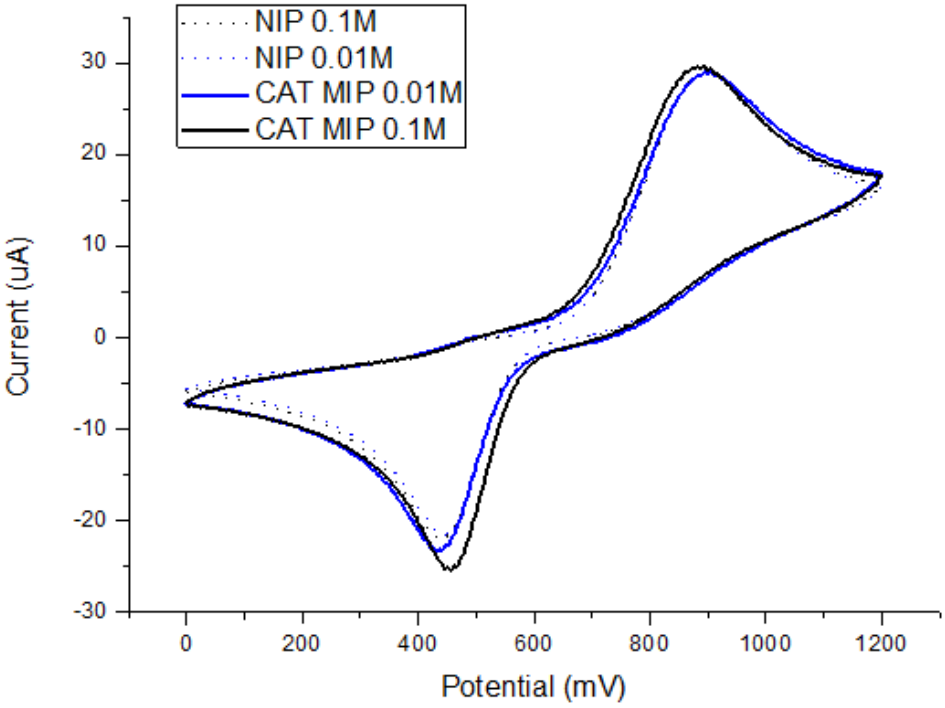

Figure 14. Comparison between concentrations of template molecule.

As a conclusion of the preliminary experiments, the final conditions to prepare MIPs were: the electrodeposition is carried out via cyclic voltammetry, applying a bias voltage from -1.5V to 0.5V, for 10 cycles at a scan rate of 0.1V/s. The chitosan solution used for the MIP contains a 0.1M of the template molecule and is adjusted to pH 4, and after electrodeposition the electrode is exposed to glutaraldehyde vapours for 20 minutes.

4.2. Sensing behaviour of MIPs based on chitosan towards compounds of interest in the food industry

4.2.1. Sensing behaviour of MIPs vs. Catechol

Once the preparation parameters were optimized the NIPs and MIPs were used to detect compounds of interest in the food industry. They included catechol, a representative of the phenols family well known for their antioxidant activity, lactic acid, an organic acid of importance in the dairy industry, and malic and tartaric acid, organic acids of interest crucial in the food industry for their roles in enhancing flavour, acting as preservative, and improving the texture and stability of various products, from beverages to baked goods.

For all the compounds under study, we will show the voltammograms corresponding to the formation of the NIP and the MIP in the presence of the template molecule, the voltammetric responses at increasing concentrations of the target molecule and the corresponding calibration curves.

Figure 15 shows the comparison between the electrodeposition of the MIP in the presence of catechol and the molecular non imprinted polymer (NIP). The **electrodeposition** was carried out using **cyclic voltammetry**, applying a varying potential from -1.5V to 0.5V, for 10 cycles. After the electrodeposition and exposition to glutaraldehyde vapours, the template molecule is eluted using a 0.1M KCl solution

As observed in the Figure 15, the voltammograms registered during the electrodeposition of chitosan in the absence or in the presence of the template molecule, show important differences. In fact, in the presence of catechol, the electrodeposition starts at lower potentials (-1200 mV for the NIP and -600 for the MIP) and attains higher intensities in

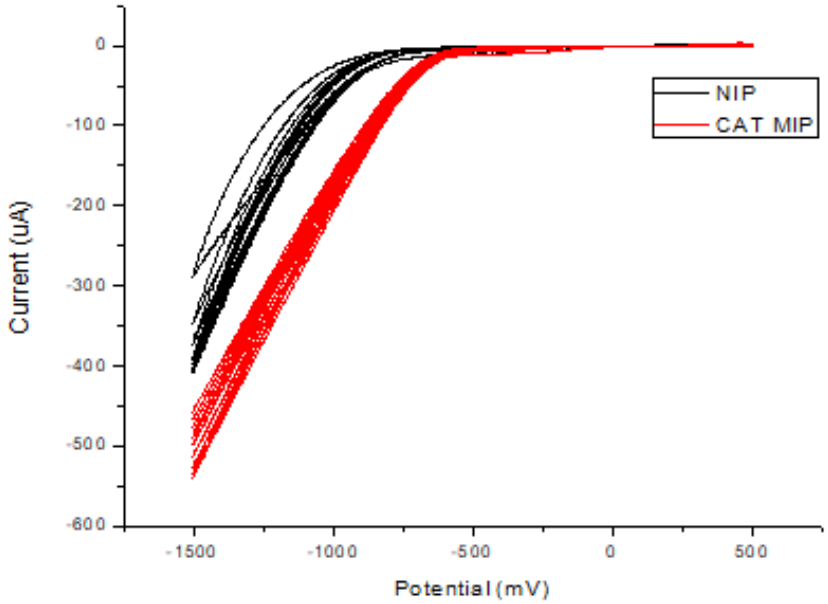

Figure 15. Electrodeposition of MIP and NIP for a catechol sensor.

absolute values (-400 μA for NIP and -600 for MIP). This effect indicates that the electrodeposition is more efficient in the presence of catechol.

Once the MIP is obtained, and the template molecule has been removed, it is time to **analyse the responses towards standard solutions of catechol**. First the response towards a 10^{-3}M catechol solution was analysed as shown in Figure 16. As stated before, both NIP and MIP show a response corresponding to the two electron oxidation reduction of catechol to the quinoid form. However, there is a clear difference of intensity between the response of the MIP and the NIP. This is caused by the presence of the holes created by the template molecule that increase the number of possible active sites.

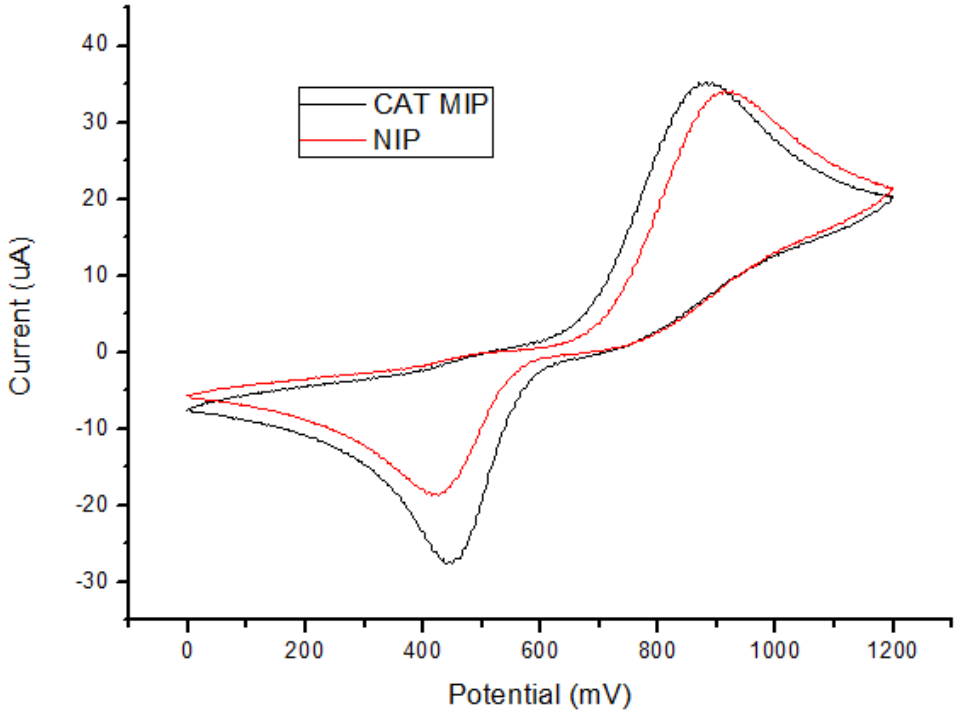

Figure 16. Electrochemical Response of MIP and NIP towards a 10^{-3} M catechol solution.

When the electrode was immersed in solutions containing increasing concentrations of catechol, the intensity of the peaks increased progressively. From these curves, it is possible to prepare a calibration curve. In this case, the calibration curve was calculated in the cathodic peak at **440 mV.** The analysis of a range of concentrations from **10^{-3}M to 10^{-6}M** gave rise to the calibration curve show in Figure 17.

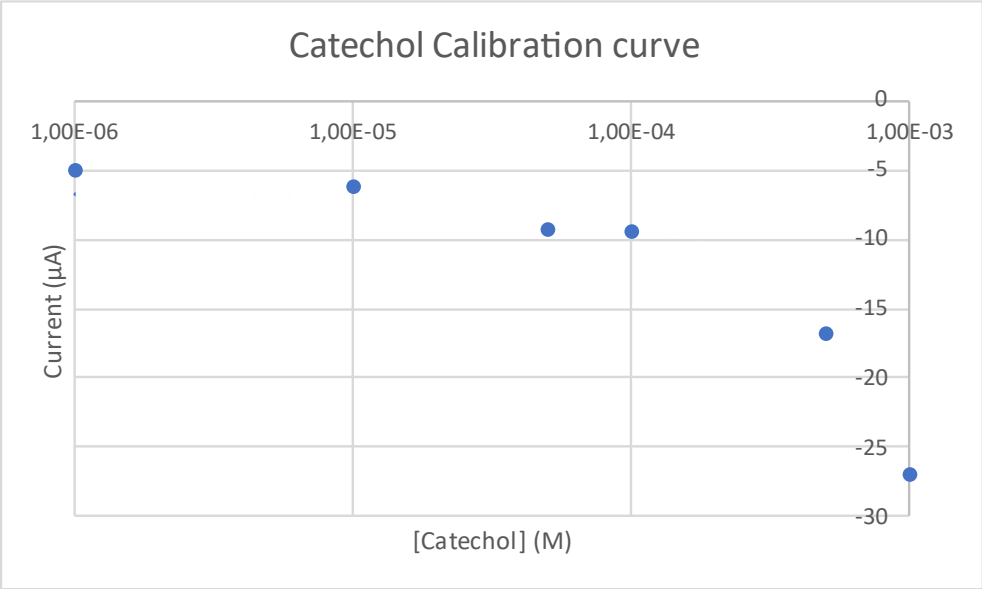

Figure 17. Catechol calibration curve. Values were obtained from the peak of the reduction curve at 440mV.

It is important to mention that the X-axis is shown in logarithmic scale for a clearer view of the graph. The curve shows the typical habit with two regions with different slope: the first region of linearity goes clearly from 10^{-3} to 10^{-4} M while the second region goes from 10^{-4} to 10^{-6} M.

Making use of the calibration curve shown above is possible to calculate the limit of detection (LOD) of the MIP sensor in the two ranges. The calculation of the limit of detection is performed using this formula:

$$LOD = \frac{3 \cdot \sigma}{slope}$$

where σ is the standard deviation, which can be calculated measuring KCl, while the slope is obtained from the calibration curve. Applying this formula, we obtain the following limit of detection:

Catechol	Slope (µA/M)	R^2	Standard deviation (µA)	LOD (M)
10^{-3}M-10^{-4}M Range	18927	0.9967	0.2339	**$3.71 \cdot 10^{-5}$**
10^{-4}M-10^{-6}M Range	44211	0.8033	0.2339	**$1.58 \cdot 10^{-5}$**

Table 1. LOD calculation for catechol sensing.

The **limit of detection** of the chitosan-based MIP sensor for the detection of **catechol** is **$3.71 \cdot 10^{-5}$ M** in the 10^{-3}M-10^{-4}M range and **$1.58 \cdot 10^{-5}$ M** in the 10^{-4}M-10^{-6}M range.

This results can be compared with various examples of sensors for the detection of catechol highlighting the diverse materials and techniques used, each with distinct linear ranges and limits of detection (LOD). One example came from the use of a sensor made with polymeric foams which presented a higher LOD, in the order of 10^{-4}M, in a linear range 2.4 to 20.0 μM.[56] Chitosan/AuNPs/Phthalocyanine composite films provided a broad linear range of 0 to 80 μM with a much lower LOD, in the order of 10^{-10}M.[57] Additionally, a nanocomposite of molecularly imprinted chitosan with carbon nanotubes and gold nanoparticles on boron-doped diamond electrodes showed a wide linear range from 0 to 1 mM and a comparable LOD, being as well in the order of 10^{-5}M.[58] Another molecularly imprinted chitosan film on boron-doped diamond electrodes was reported without the use of any other nanostructure, this sensor presented a linear range from 0 to 80 μM with a detection limit in the order of 10^{-7}M.[59]

The molecularly imprinted chitosan film on glassy carbon electrodes stands out for its competitive sensitivity and broad detection range, particularly excelling in the lower concentration ranges compared to the other materials and methods. Although the LOD is not the best, its limit of detection is in the order of 10^{-5}M for a range from 10^{-3}M to 10^{-6}M and presents the advantage that it can be easily prepared making it particularly interesting.

The next step will be to synthesize sensors for the detection of organic acids that are important in the food industry, such as lactic, malic and tartaric acid. The parameters obtained from the catechol study will be applied for the next template molecule studies.

4.2.2. Sensing behaviour of MIPs vs. Lactic acid

Lactic acid is an organic acid (**pKa=3.86**)[60] with multiple significant uses in food industry, it is considered a very important additive since it has multiple applications from pH regulation to flavouring properties (Figure 18). Lactic acid plays a key role in **fermented food** products such as wine, fermented milks or vegetables.[61]

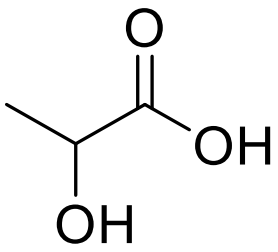

Figure 18. Lactic acid structure.

A chitosan based MIP sensor for the detection of lactic acid was prepared making use of the optimized parameters from section 4.1. The electrodeposition of this sensor was carried out using a **0.1M concentration** of lactic acid dissolved in chitosan solution as shown in Figure 19.

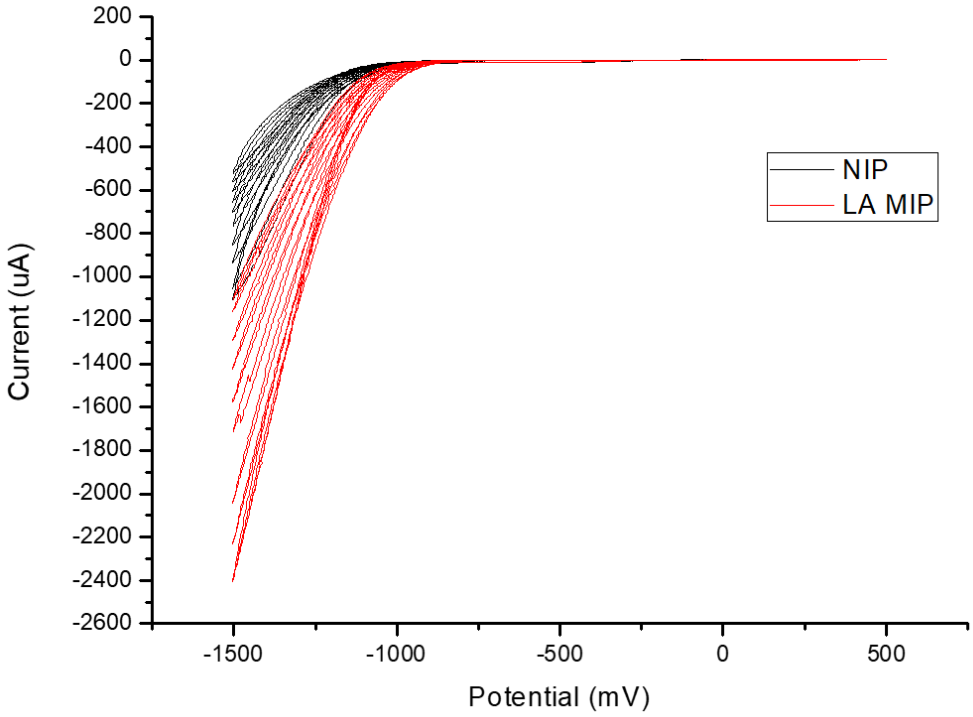

Figure 19. Electrodeposition of chitosan based MIP sensor for lactic acid.

In this case, electrodeposition started at the same potential for NIP and for MIP. In these conditions the lactic acid caused a progressive decrease of the intensity that for the MIP ranged from -1200 to -2400 µA. As these values are higher than the intensity values observed during electrodeposition of catechol, it can be concluded that lactic acid

facilitates the electrodeposition process. Also in this conditions, there is a clear difference in the intensity produced during the electrodeposition that occurred in the presence and in the absence of the template molecule.

After the elution of the lactic acid from the MIP, the electrochemical response of both electrodes (NIP and MIP) was tested by immersing the electrodes in a **10^{-3}M solution of lactic acid** in 0.1M KCl.

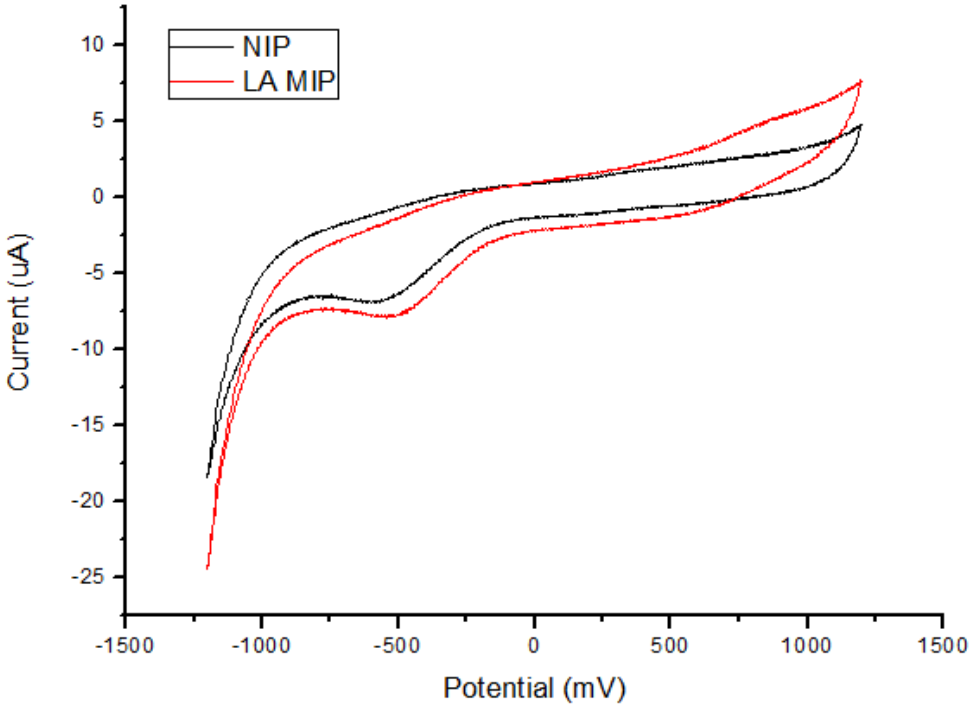

Figure 20. Cyclic voltammogram of NIP and MIP for the analysis of 10^{-3}M lactic acid solution.

Figure 20 shows the responses of both electrodes. A peak specific for lactic acid is not observed since this compound does not have electroactivity in the studied range. The responses were characterised by a cathodic peak at ca. -500 mV that is attributed to the reduction of oxygen present in the solution. Only slight differences between the intensity of response of NIP and MIP can be observed, indicating that the molecular imprinting was not efficient under these conditions.

Taking this into account, the preparation conditions were modified, decreasing the concentration of template molecule to **10^{-4}M of lactic acid**.[62] Figure 21 showed that the electrodeposition process was better controlled.

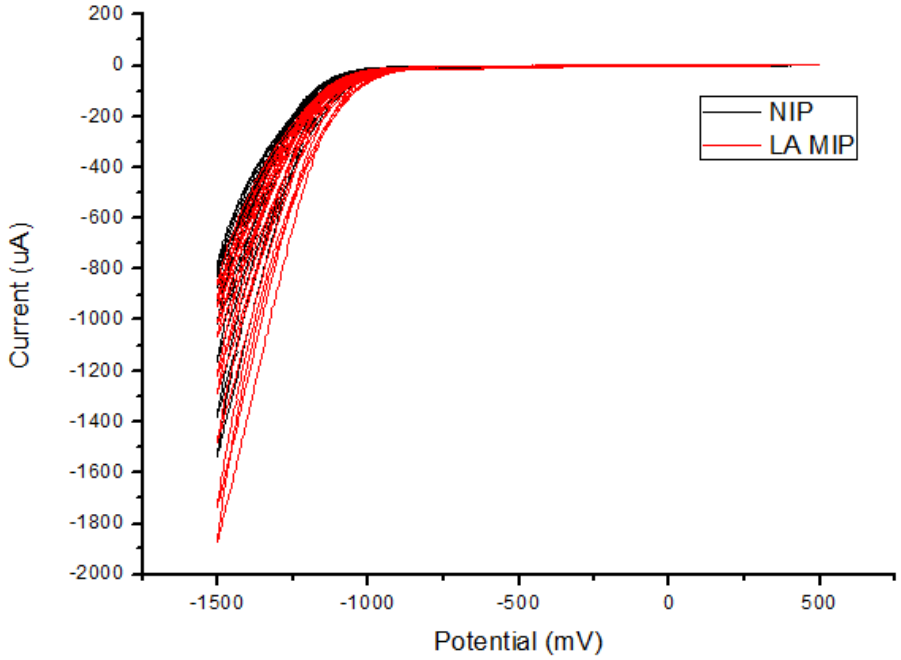

Figure 21. Electrodeposition of 10^{-4}M lactic acid CS solution (MIP).

The change in the deposition conditions was very effective and the responses of MIPs prepared using a lower concentration of the template gave more intense responses to lactic acid that the NIP (Figure 22). This can be interpreted in terms of a better control of the electrodeposition that produces better imprints.

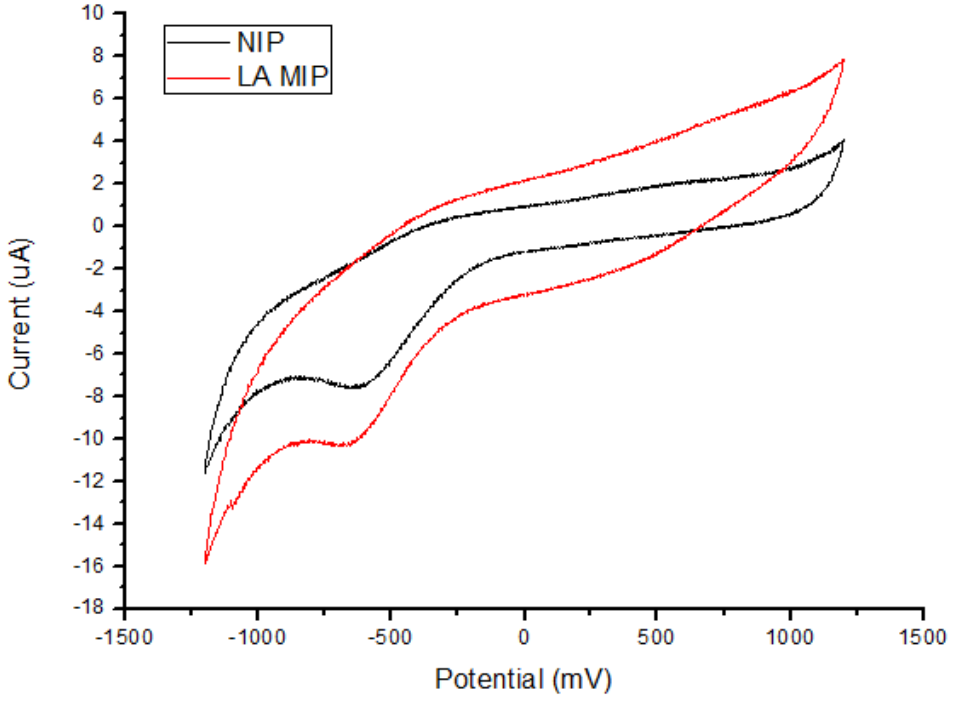

Figure 22. Analysis of the response of a MIP and a NIP immersed in a 10^{-6}M lactic acid solution.

Therefore, the optimised sensor prepared with lower concentration of the template (10^{-4} M) was used in further experiments.

In order to construct the **calibration curve**, lactic acid solutions from a range of **10^{-3}M to 10^{-11}M** were analysed. In the case of this acidic solution, the increase in the concentration of the lactic acid, produced a decrease in the intensity of the redox peak at ca. **-650 mV** (Figure 22). This peak can correspond to the **reduction of O_2**.[63] The overall reactions for Oxygen Reduction in acidic and alkaline solutions are as following

$$O_2 + 4H^+ + 4e^- \rightleftarrows 2H_2O$$

$$O_2 + 2H_2O + 4e^- \rightleftarrows 4OH^-$$

This reaction produces the interfacial pH to move in a basic direction. Afterwards the interfacial hydroxide dissipates through a process of diffusion controlled neutralization.

The reduction of O_2 takes place at the electrode surface, and it is altered by the presence of protons. The presence of protons interferes in the reduction of oxygen since they adsorb to the electrode surface, hindering the adsorption of O_2 and thus its reduction.[64]

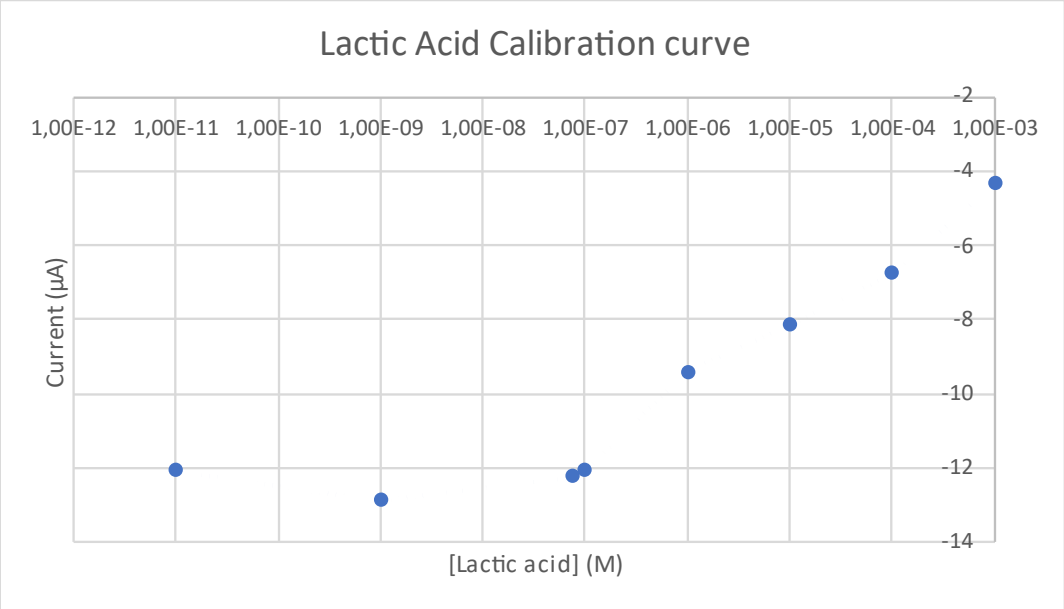

Figure 23. Lactic acid MIP sensor calibration curve for the detection of lactic acid.

Figure 23 shows the calibration curve obtained for the chitosan-based MIP sensor for the detection of lactic acid. The X-axis is shown in logarithmic scale for a clearer view of the graph. Figure 23 shows a plateau in concentrations lower than $5 \cdot 10^{-7}$M, and also presents two different linear regions, being the first one from the range 10^{-3}M to 10^{-6}M and the other one from 10^{-6}M to 10^{-9}M.

Using the information obtained from the calibration curve and the formula shown previously, the limit of detection can be calculated for both linear regions, as shown in table 2.

Lactic Acid	Slope (µA/M)	R^2	Standard deviation (µA)	LOD (M)
10^{-3}M-10^{-6}M Range	4070	0.8206	0.3532	$2{,}60 \cdot 10^{-4}$
10^{-6}M-10^{-9}M Range	3024209	0.9275	0.3532	$3{,}50 \cdot 10^{-7}$

Table 2. Limit of detection obtained for the lactic acid chitosan-based MIP sensor

Limits of detection obtained for the chitosan-based MIP sensor prepared for **lactic acid** sensing presented a good order of magnitude in their respective linear ranges, highlighting the one obtained in the lower concentrations range, being in the order of **10^{-7}M**.

4.2.3. Sensing behaviour of MIPs vs. Malic acid

Malic acid is an organic acid (**pKa_1= 3.46, pKa_2= 5.05**)[1] present in some vegetables and specially fruits such as grapes. It plays a key role in wine being one of the predominant sources of acidity, affecting multiple levels of the **winemaking** process and lately the wine quality speaking of organoleptic properties and perception.[65]

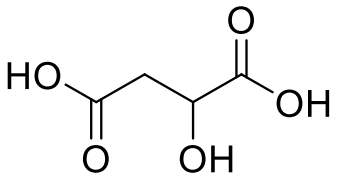

Figure 24. Malic acid structure

A chitosan-based MIP sensor for the detection of **malic acid** has been prepared. In order to obtain this sensor a **0.1M malic acid** chitosan solution has been electrodeposited using cyclic voltammetry and the parameters described in section 4.1. The electrodeposition is shown in Figure 25.

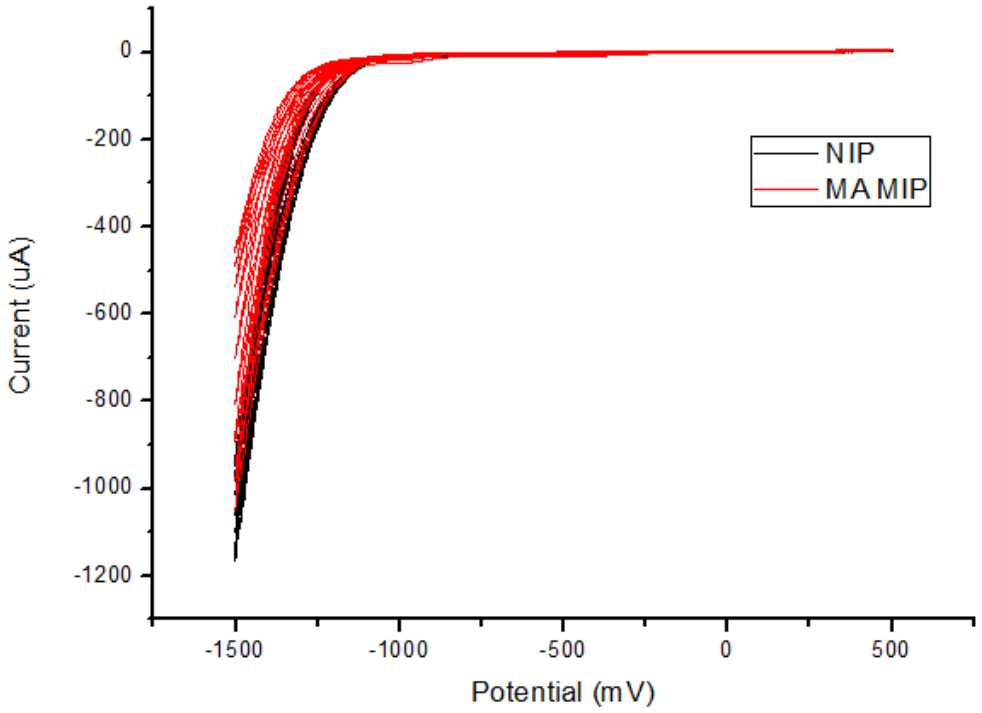

Figure 25. Electrodeposition in a 0.1M malic acid (MIP) and in absence of malic acid (NIP).

After the electrodeposition and the corresponding procedures, a **10^{-3}M malic acid solution** was analysed, once again via cyclic voltammetry.

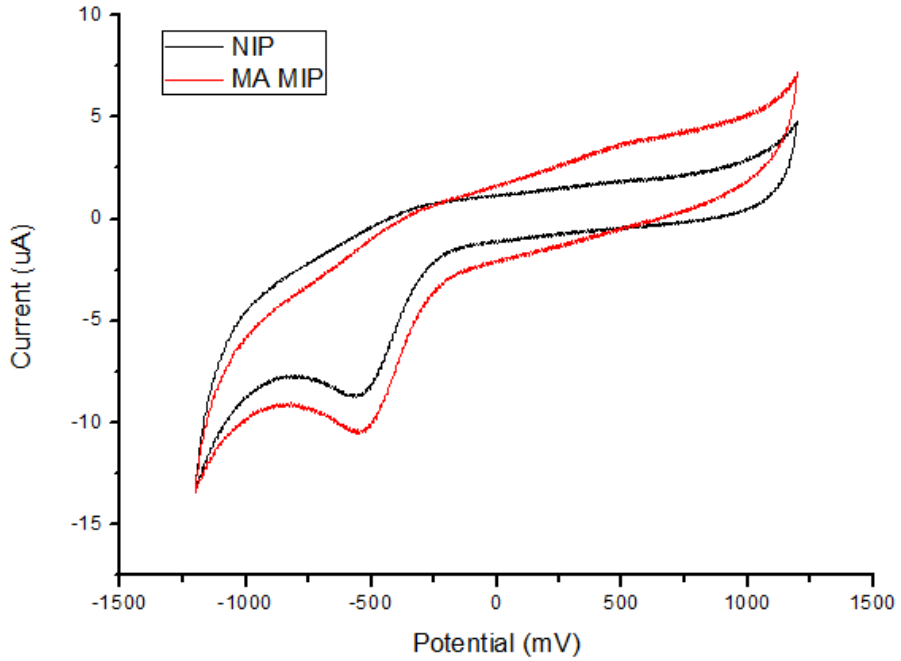

Figure 26. Cyclic voltammogram of the response of the MIP and NIP to a 10^{-3}M malic acid solution.

The shape of the voltammograms is similar to that observed in lactic acid, confirming that the redox peaks observed are related to the oxygen. Figure 26 shows a comparison between the MIP and the NIP, the cyclic voltammogram shows that the MIP intensity of response increases hugely in comparison with the NIP.

The next step is to construct a **calibration curve**, in order to do so multiple solutions with a range of concentrations from **10^{-3}M to 10^{-7}M** have been analysed employing cyclic voltammetry. The X-axis is shown in logarithmic scale for a clearer view of the graph.

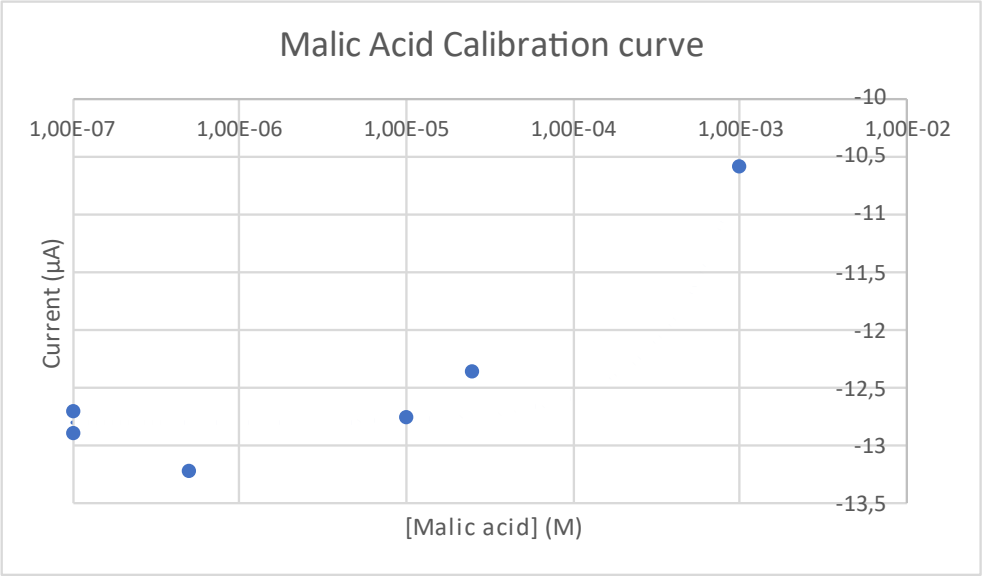

Figure 27. Malic acid calibration curve. Values were obtained from the peak of the reduction curve at -550mV.

The calibration curve shows a linear range between the concentrations 10^{-3}M to $5 \cdot 10^{-7}$M, so the limit of detection is calculated in this range, using the information provided by the linear adjustment. The adjustment of lower concentrations has a terrible R^2 coefficient, thus the limit of detection in that range is not calculated.

Malic Acid	Slope (µA/M)	R^2	Standard deviation (µA)	LOD (M)
10^{-3}M-$5 \cdot 10^{-7}$M Range	2228.1	0.9185	0.0204	**$2.75 \cdot 10^{-5}$**

Table 3. LOD calculation for malic acid sensing.

The **limit of detection** (LOD) for the chitosan-based MIP sensor for the detection of **malic acid** is **$2.75 \cdot 10^{-5}$ M**, in the linear range from 10^{-3}M to $5 \cdot 10^{-7}$M.

4.2.4. Sensing behaviour of MIPs vs. Tartaric acid

Tartaric acid is an organic acid (**pKa_1= 3.04, pKa_2= 4.37**)[1] used in various industries, including as an acidifier, antioxidant, and flavour enhancer in winemaking. It is also utilized in the food, bakery, and pharmaceutical sectors. This acid is a significant low molecular weight component in both red and white **wines**. Its concentration in grape juices and wines is critical to monitor, as it affects the taste, stability, and microbiological characteristics of these drinks.[66,67]

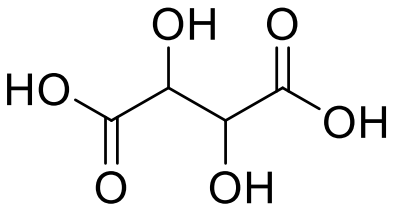

Figure 28. Tartaric acid structure.

A chitosan-based MIP sensor for the detection of **tartaric acid** has been prepared by the **electrodeposition** of a **0.1M tartaric acid** chitosan solution using cyclic voltammetry and the parameters described in section 4.1.

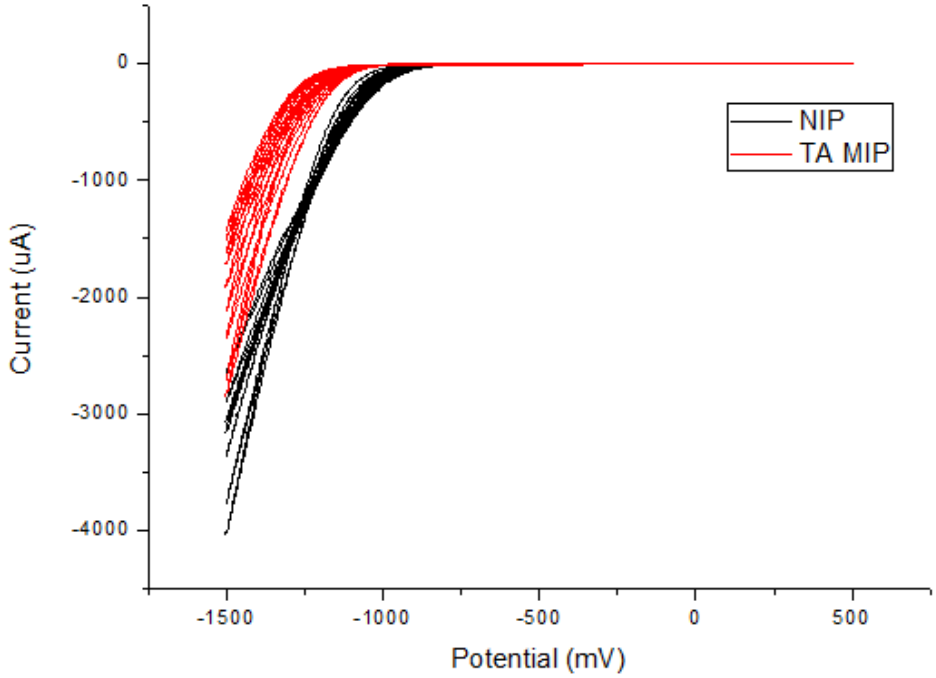

Figure 29. Chitosan electrodeposition in tartaric acid 0.1M.

Figure 29 shows the electrodeposition of both MIP and NIP, this time the NIP reaches higher values of current in comparison with the MIP. This can be due to the presence of 0.1M tartaric acid in the chitosan solution electrodeposited on the MIP electrode.

After the electrodeposition, a **10^{-3}M tartaric acid** solution in 0.1M KCl was analysed via cyclic voltammetry, as shown in Figure 30.

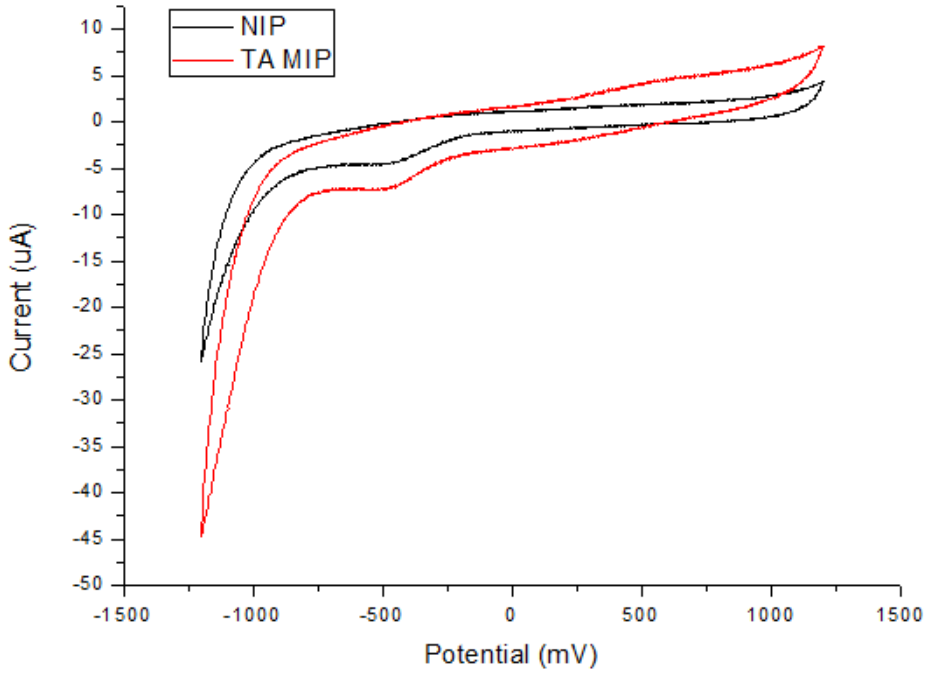

Figure 30. Cyclic voltammogram of the analysis of a 10^{-3}M tartaric acid solution.

Once again, after checking that the intensity of response of the MIP is higher than that for the NIP, a **calibration curve** is prepared. This time solutions with a range of concentrations from **10^{-3}M to 10^{-11}M** of **tartaric acid** were prepared and consequently analysed via cyclic voltammetry. The resulting calibration curve can be observed in Figure 31.

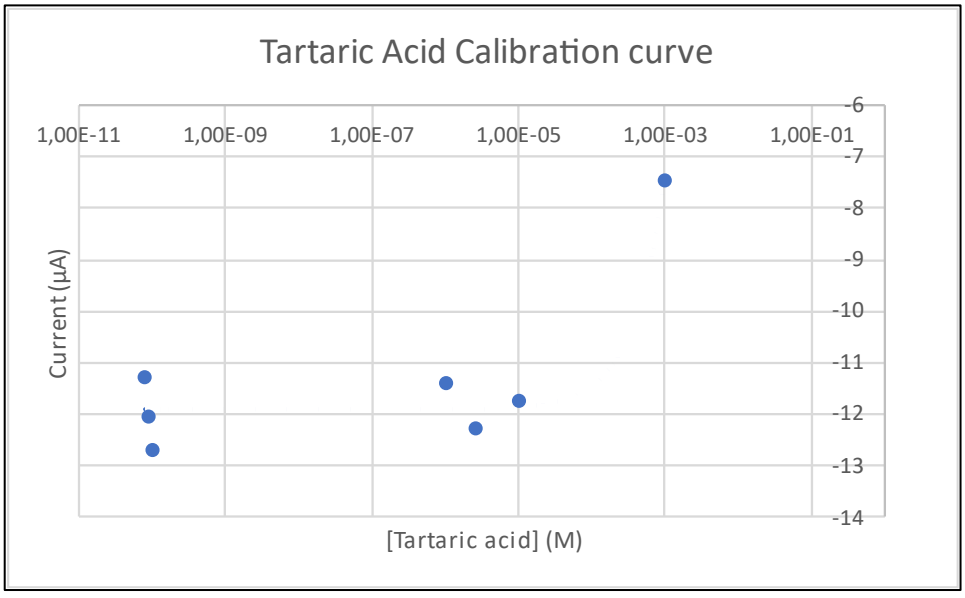

Figure 31. Calibration curve for the detection of tartaric acid.

The calibration curve provides the information needed to calculate the limit of detection of the tartaric acid sensor. The calibration curve shows two regions, one in higher concentrations from 10^{-3}M to 10^{-6}M, and another region in lower range of concentrations from 10^{-6}M to $8 \cdot 10^{-11}$M, this last one presents bad linearity which is the reason why the

limit of detection is not calculated in this region. The limit of detection is calculated in Table 4.

Tartaric Acid	Slope (µA/M)	R^2	Standard deviation (µA)	LOD (M)
10^{-3}M-10^{-6}M Range	4363.4	0.9734	0.0680	**$4.67 \cdot 10^{-5}$**

Table 4. LOD calculation for tartaric acid sensing

The limit of detection for the chitosan-based MIP sensor for the detection of tartaric acid is **$4.67 \cdot 10^{-5}$M** for the range of concentrations 10^{-3}M to 10^{-6}M of tartaric acid. Once again the obtained result is a limit of detection in the order of 10^{-5}M, which is a more than considerable value for the sensing of tartaric acid in the food industry.

4.3. Selectivity Assays for Chitosan-based MIP sensors

As explained before, the principle of detection with MIPs is the creation of holes or imprints with a template molecule that can induce selectivity in the electrochemical response.

The next step of this work was to evaluate the level of selectivity of the MIP sensors, therefore the cross selectivity of the different organic acids included in the study was evaluated. For this purpose, the MIP prepared in the presence of malic acid was immersed in solutions of the other acids (lactic and tartaric acid), the NIP was also immersed in those solutions to take into account the unspecific response.

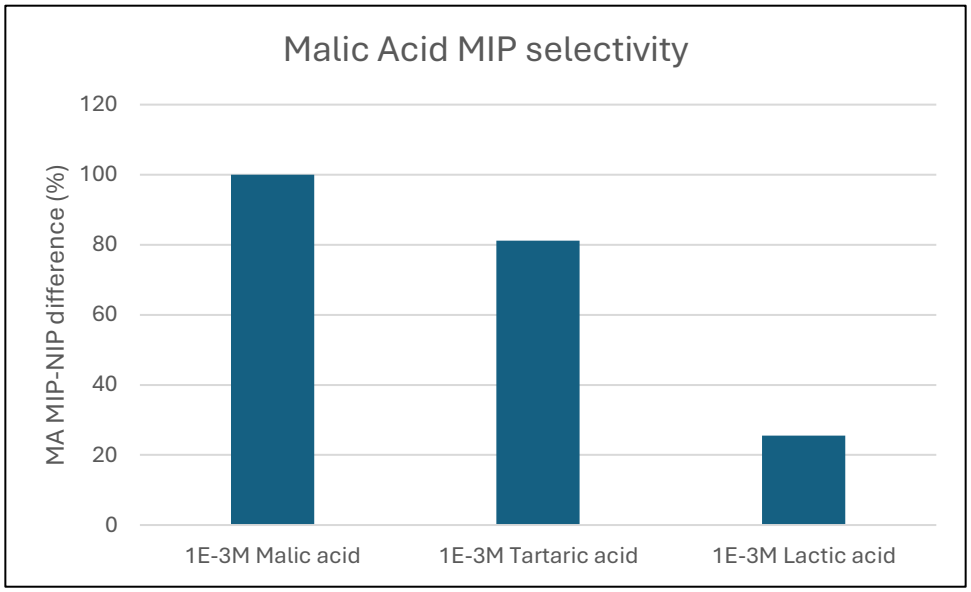

Figure 32. Percentage of difference of intensity of response between the malic acid MIP and the NIP when immersed in: 10^{-3}M malic acid solution(left), 10^{-3}M tartaric acid solution (middle) and 10^{-3}M lactic acid solution (right).

The responses are presented as the difference (expressed in percentage) between the results obtained with the MIP and the NIP. Showing the results in this way we can observe easily the percentage of specific response, which corresponds to the interaction with the specific recognition cavities presented in the MIP.

The difference of response for the case of **malic acid** is the biggest one, thus considered the maximum specific response and therefore it is taken as the reference (100%).

The case of **tartaric acid** shows the limitations of the molecular imprinting polymers technique as tartaric acid and malic acid have almost the exact same structure, lacking this last one an hydroxyl group to be identical. This similarity leads the malic acid MIP to present a considerable specific recognition towards tartaric acid (80%), considering then that tartaric acid is able to partially interact with the created specific recognition cavities.

When immersing the electrodes in a 10^{-3}M **lactic acid** solution the difference of response is up to just a 25%. This result is especially good and means that the specific cavities designed using malic acid as template molecule almost does not interact with lactic acid, despite the similarity of structure between malic and lactic acid.

This results show that the molecular imprinting polymers technique, although it has some limitations, allows to discriminate between complex molecules given enough differences related to their structure and size.

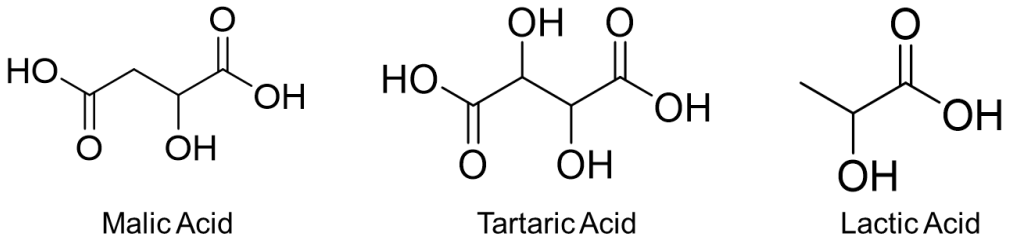

Figure 33. Structure of malic acid (left), tartaric acid (middle) and lactic acid (right).

4.4. Improvement of the performance by addition of metallic nanoparticles

It is well known that metallic nanoparticles such as AuNPs or AgNPs have an electrocatalytic effect due to the reactivity of their surfaces usually linked to the existence of mixed valence states.[68,69] For this reason, an attempt was made to improve the intensity of the signals by introducing AuNPs or AgNPs in the structure of the MIPs.

Aqueous **gold nanoparticles (AuNPs)** were prepared via reduction of **tetrachloroauric acid** ($HAuCl_4$) using **sodium citrate**. This solution was mixed with the 1.5 mg/mL chitosan solution with a **1:2 AuNPs:CS** volume ratio. Aqueous **silver nanoparticles** (**AgNPs**) were prepared by the **reduction of $AgNO_3$** with **$NaBH_4$** at low temperature. The AgNPs solution was mixed with the chitosan solution in a **1:2 AgNPs:CS** volume ratio.

4.4.1. Chitosan/MNPs based MIP for catechol detection

The addition of **gold nanoparticles** or **silver nanoparticles** to a **0.1M catechol** chitosan solution follows the normal parameters described in section 4.1. and presents the following results.

Figure 34 shows the **electrodeposition** of both NIP and MIP, both containing AuNPs (a), AgNPs (b) and chitosan. The solution used for the preparation of the MIP contains also a concentration of 0.1M in catechol.

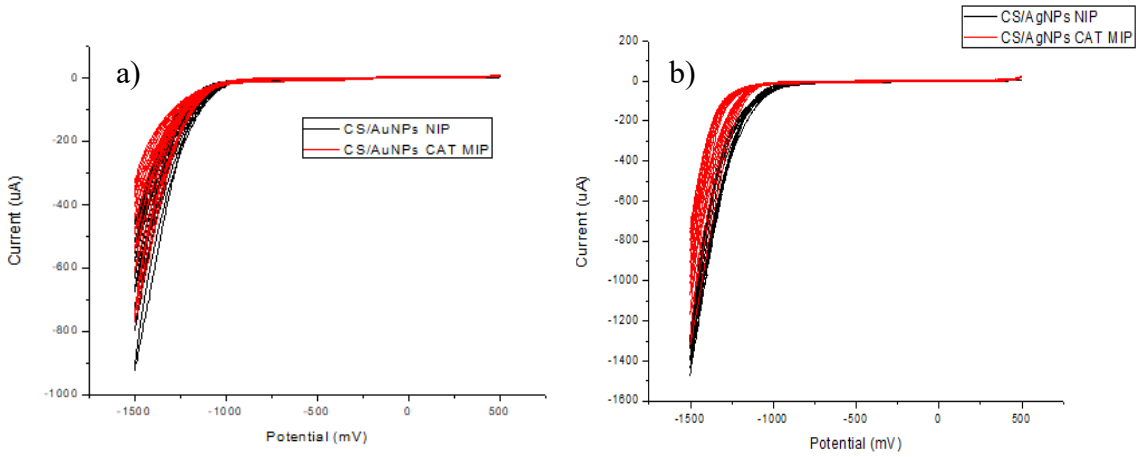

Figure 34.a) Electrodeposition of CS/AuNPs solution (NIP)and CS/AuNPs catechol solution (MIP). b)Electrodeposition of CS/AgNPs solution (NIP) and CS/AgNPs catechol solution (MIP).

The shape of the curves obtained during the electrodeposition are similar to those obtained in the absence of AuNPs, but the presence of nanoparticles, increased the intensity of the current, probably due to an enhancement of the conductivity of the solution. Once prepared the MIP sensors, the response was tested analysing a **10^{-3}M catechol** solution via cyclic voltammetry.

The MIP doped with AuNPs (Figure 35a) shows a cathodic peak at approximately **380 mV**, this peak corresponds to the **reduction of catechol**. Initially this peak was observed at around 440 mV, the displacement to lower potential is due to the **electrocatalytic effect** of **AuNPs**. The MIP doped with AgNPs (Figure 35b) shows a peak at approximately **290mV**, once again this peak is assigned to the reduction of the quinoid form to catechol. The displacement of this peak to a lower potential can be explained due to the presence of **silver nanoparticles** that exert an electrocatalytic effect. MIP shows a much higher intensity of response in comparison to the non-imprinted polymer.

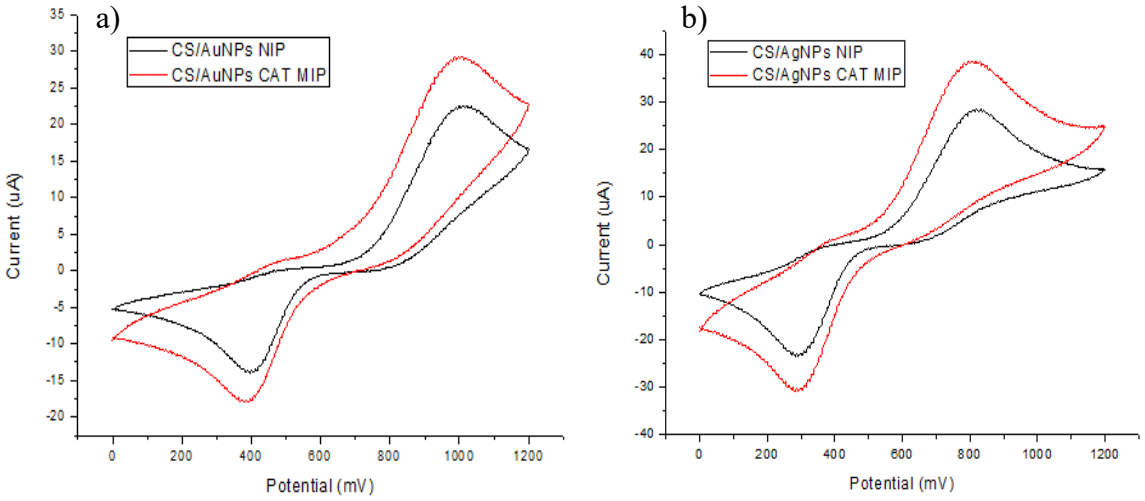

Figure 35. Comparison between NIP and MIP response to a 10^{-3}M catechol solution for the CS/AuNPs sensor (a) and the CS/AgNPs sensor (b).

After studying the effects of the addition of both **gold** and **silver** nanoparticles, it is important to compare their results between each other and also with the **non-addition** of nanoparticles, previously shown in section 4.2. To perform this **comparison**, the data from the analysis of a **10^{-3}M catechol solution** is taken, and the graphic comparison shown in Figure 36 is obtained. As it was previously mentioned in both **AuNPs** and **AgNPs** the **peak** for the **reduction of catechol** suffers a displacement to lower potentials due to the electrocatalytic effects of the metallic nanoparticles. This **displacement** is more relevant in the case of AgNPs.

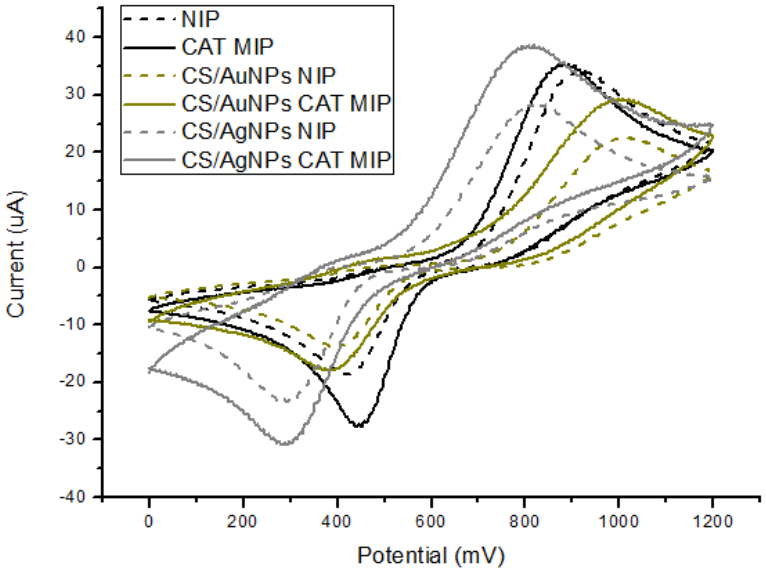

Figure 36. Comparison of MIP and NIP with the addition or not of metallic nanoparticles. Figure shows the response of the different sensors prepared to a 10^{-3}M catechol solution.

A **calibration curve** was prepared for each sensor, one for the use of **AuNPs** and another one for **AgNPs**. Both calibration curves were obtained from the analysis of a range of concentrations from **10^{-3}M to 10^{-6}M in catechol**. The limit of detection of the **CS/AuNPs** MIP sensor for the detection of **catechol** is **$8.28 \cdot 10^{-5}$M**. The limit of detection of the **CS/AgNPs** MIP sensor for the detection of **catechol** is **$2.18 \cdot 10^{-5}$M**.

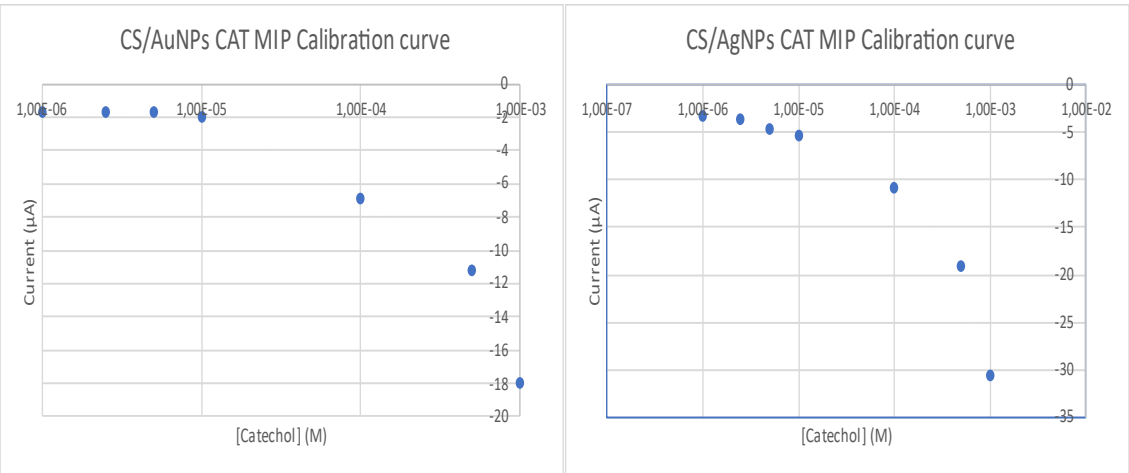

Figure 37. Calibration curves for the detection of catechol with the chitosan sensor with AuNPs(left) or with AgNPs (right).

The two calibration curves in Figure 37 present clearly two different regions, in both sensors there is a region from 10^{-3}M to 10^{-5}M catechol and another region that goes from a 10^{-5}M to 10^{-6}M catechol. Figures 38 and 39 show a zoom-in of these two regions for the CS/AuNPs MIP sensor and the CS/Ag NPs MIP sensor respectively.

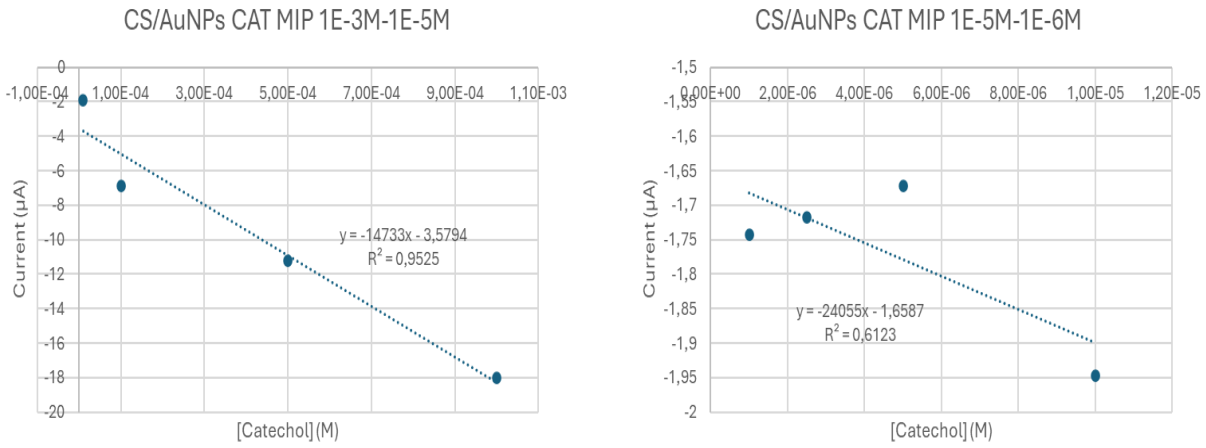

Figure 38. Zoom-in of the different regions present in the CS/AuNPs CAT MIP calibration curve.

Figure 38 shows that the region from 10^{-5}M to 10^{-6}M obtained from the CS/AuNPs MIP has a really low value of the R^2 coefficient, this has to be considered before adding AuNPs to the chitosan MIP.

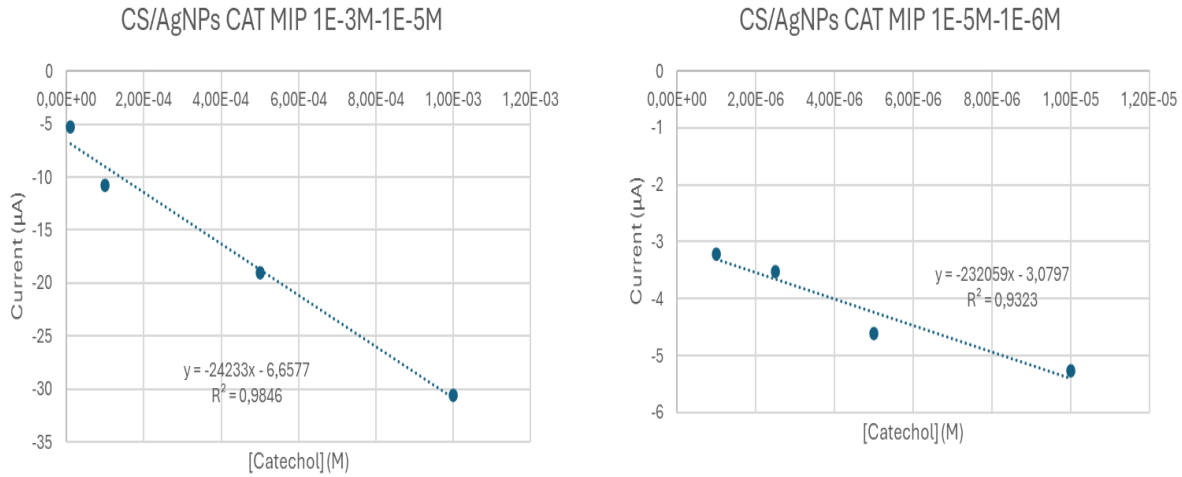

Figure 39. Zoom-in of the different regions present in the CS/AgNPs CAT MIP calibration curve.

Figure 39 shows both linear regions present in the CS/AgNPs MIP sensor calibration curve. In contrast to Figure 38, it shows high values of the R^2 coefficient in both concentrations ranges.

Calibration curves provide the information required to calculate the limit of detection of each sensor for catechol detection. Table 5 shows the limit of detection for the different types of chitosan-based MIP sensor prepared for the detection of catechol in the range of 10^{-3}M to 10^{-5}M concentration of catechol.

Catechol (10^{-3}M-10^{-5}M range)	Slope (µA/M)	R^2	Standard deviation (µA)	LOD (M)
Chitosan	18927	0.9967	0.2339	**$3.71 \cdot 10^{-5}$**
CS/Au NPs	14733	0.9525	0.4504	**$9.17 \cdot 10^{-5}$**
CS/Ag NPs	24233	0.9846	0.1571	**$1.94 \cdot 10^{-5}$**

Table 5. Limit of detection in the range of 10^{-3}M-10^{-5}M catechol concentration for the different chitosan-based MIP sensors prepared for catechol sensing.

Table 6 shows the limit of detection for the different types of chitosan-based MIP sensor prepared for the detection of catechol in the range of 10^{-5}M to 10^{-6}M concentration of catechol.

Catechol (10^{-5}M-10^{-6}M range)	Slope (µA/M)	R^2	Standard deviation (µA)	LOD (M)
Chitosan	44211	0.8033	0.2339	**$1.58 \cdot 10^{-5}$**
CS/Au NPs	24055	0.6123	0.4504	**$5.62 \cdot 10^{-5}$**
CS/Ag NPs	232059	0.9323	0.1571	**$2.03 \cdot 10^{-6}$**

Table 6. Limit of detection in the range of 10^{-5}M-10^{-6}M catechol concentration for the different chitosan-based MIP sensors prepared for catechol sensing.

Figure 36, Table 5 and Table 6 give information about the **intensity of response** and the **limit of detection** of each sensor.

In the case of **gold nanoparticles,** the intensity of response decreases while LOD increases in comparison to the non-use of metallic nanoparticles. Also, the study of the linear range from lower concentrations, 10^{-5}M to 10^{-6}M, gives a low R^2 coefficient, which translates into the obtention of inconsistent results when adding AuNPs. All of this reasons are more than enough to **stop** the use of AuNPs in the preparation of future chitosan-based MIP sensors.

The use of **silver nanoparticles increases** the **intensity of response** of both NIP and MIP, keeping similar differences between the intensity of response of both of them, as well as decreases the **limit of the detection**. The increase of the intensity of response makes the addition of metallic nanoparticles to the chitosan-based MIP an adequate strategy to improve the performance of the MIP sensors.

From the above results it could be concluded that the AgNPs were a more efficient electrocatalyst than AuNPs. For this reason, the use of AuNPs was discarded and the work continued centered in AgNPs.

4.4.2. Chitosan/AgNPs based MIP sensor for the detection of organic acids

The addition of **silver nanoparticles** to organic acid chitosan-based MIP sensors was also performed for the detection of **tartaric acid**. Tartaric acid was chosen as a representative of the organic acids due to the similarity of its structure to both of the other organic acids presented before (lactic and malic acid). The preparation of the CS/AgNPs MIP starts with the electrodeposition of the chitosan solution, which presents a 1:2 AgNPs:CS volume ratio.

The electrodeposition is shown in Figure 40, in the specific case of MIP the CS/AgNPs solution also contains a concentration of **0.1M of tartaric acid**.

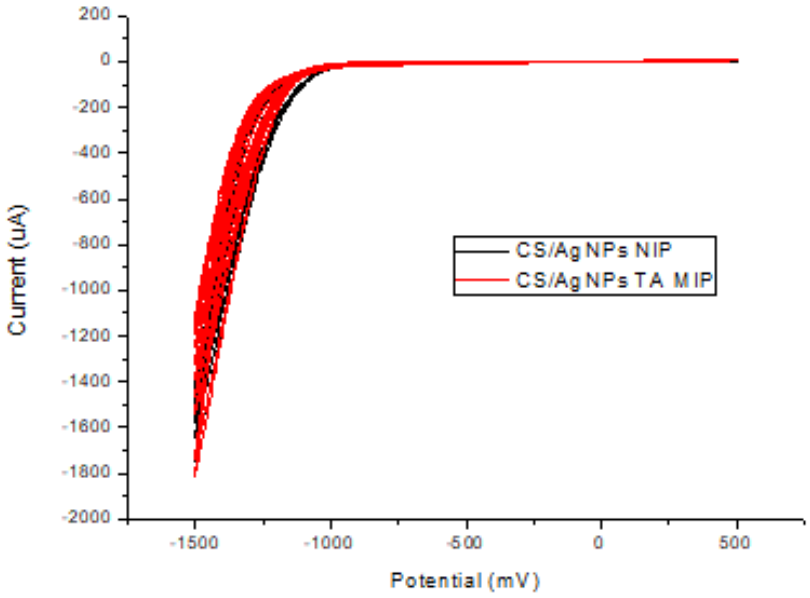

Figure 40. Electrodeposition of CS/AgNPs solution , in the case of MIP containing a 0.1M tartaric acid concentration.

The next step was to analyse a **10^{-3}M tartaric acid** solution via cyclic voltammetry, as shown in figure 41.

It can be observed that the peak at around **-500mV** that was attributed to reaction of oxygen with H^+ has a much higher intensity of response in MIP than in NIP. (Notice that a very small peak observed in the anodic wave at ca. 300 mV corresponds to the one electron oxidation of metallic silver to Ag^+.[70] This peak was not observed in catechol because it was overlapped with the catechol oxidation).

The formation of OH^- can induce a change of the interfacial pH, and its neutralization can occur with the interaction of the lactic acid molecules present in the electrode. In the case of the NIP all these acid molecules are present in the surface while in the case of MIP, there will be also acid molecules in the specific cavities created during the MIP formation. Consequently, there is no interaction with the acid molecules present in this holes, since the surface acids act blocking the access, this could explain why there is a higher intensity of response in the MIP.

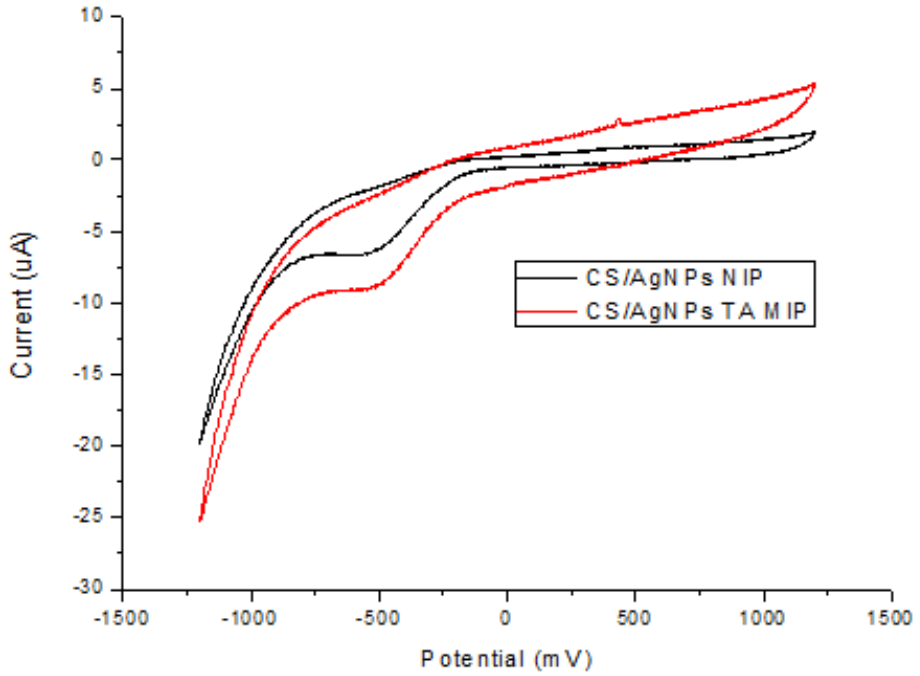

Figure 41. Analysis of the response of the CS/AgNPs sensor to a 10^{-3}M tartaric acid solution.

Figure 42 shows a **comparison** between the use of AgNPs and the non-use of nanoparticles, it can be noticed that the **intensity** of response of both NIP and MIP **increases** considerably, but the difference of intensity between both of them remains similar.

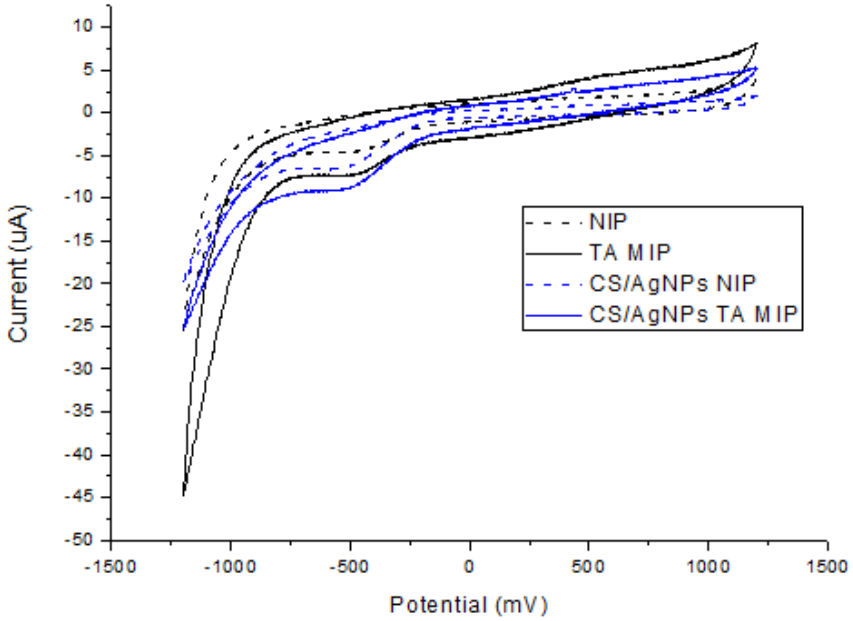

Figure 42. Comparison between the use of AgNPs or non-use for the response to a 10^{-3}M tartaric acid solution.

A calibration curve for the AgNPs chitosan-based sensor was prepared analysing a range of solutions with concentrations from 10^{-3}M to 10^{-6}M of tartaric acid. Figure 43 shows the obtained calibration curve.

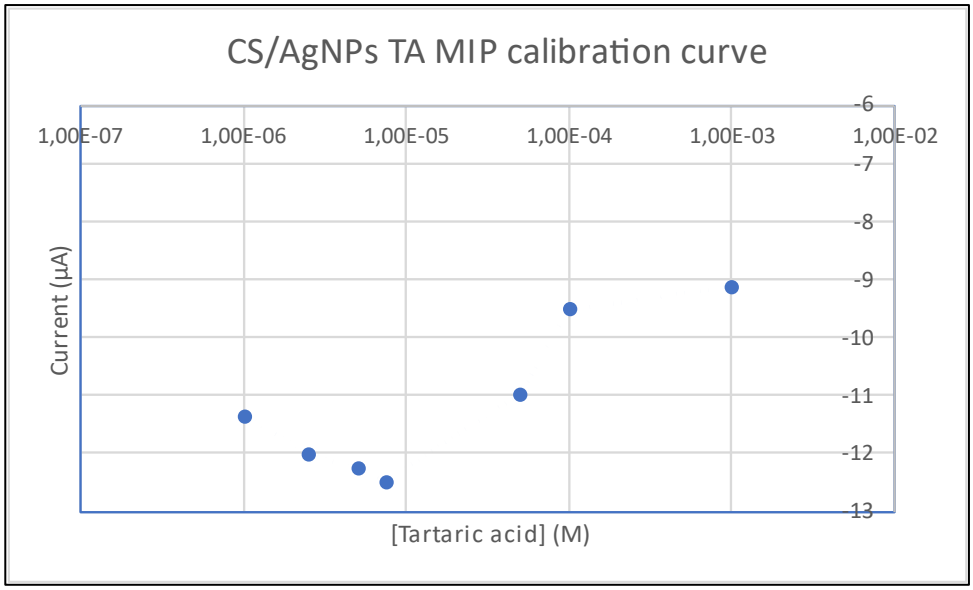

Figure 43. Calibration curve of the CS/AgNPs TA MIP for the detection of tartaric acid.

The prepared calibration curve shows two different regions, one from 10^{-3}M to 10^{-5}M and another from 10^{-5}M to 10^{-6}M. Figure 44 shows zoom-in of both regions, in the left part of the figure we can see that the R^2 coefficient obtained for the analysis of the higher range of concentrations is pretty low.

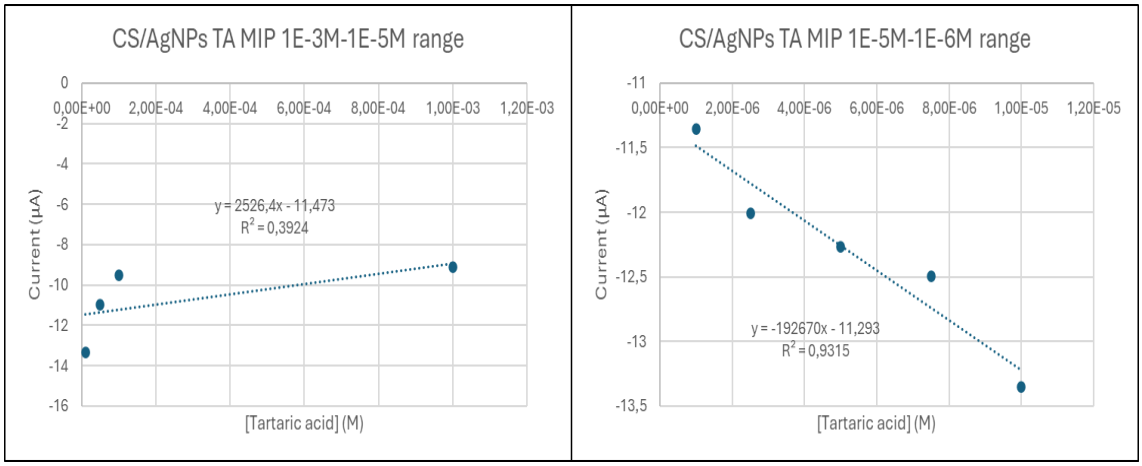

Figure 44. Zoom-in of the different regions of the CS/AgNPs MIP sensor for tartaric acid.

The required information to calculate the limit of detection of the sensor for tartaric acid in each linear range can be obtained from the calibration curve. The limit of detection from the range 10^{-3}M to 10^{-5}M is not calculated as there is almost no linearity.

Tartaric acid	Slope (µA/M)	R^2	Standard deviation (µA)	LOD (M)
CS/AgNPs MIP (10^{-5}M-10^{-6}M Range)	192670	0.9315	0.3357	**$5.23 \cdot 10^{-6}$**
MIP (10^{-3}M-10^{-6}M Range)	4363.4	0.9734	0.0680	**$4.67 \cdot 10^{-5}$**

Table 7. Limit of detection for the different chitosan-based MIP sensors prepared for tartaric acid sensing.

Table 7 shows the calculated limit of detection for the different chitosan-based MIP sensors prepared for the detection of tartaric acid. Results show that the addition of AgNPs to the chitosan-based MIP sensor decreases the limit of detection in certain linear ranges as it allows to obtain higher intensity of response.

However, it is also really important to mention that the difference between the limit of detection of both sensors is just one order of magnitude, an even more important is to mention how the values of the standard deviation get much higher when using silver nanoparticles. The use of silver nanoparticles, even though it increases the intensity of response, is not positive due to its inconsistency as show in the lack of linearity in the range of 10^{-3}M-10^{-5}M concentration of tartaric acid and in the value of the standard deviation obtained for the prepared sensor. Another important thing to mention is the added cost of the addition of silver nanoparticles, as well as the environmental inconveniences that its use may present.

All the statements mentioned before lead to the conclusion that the addition of AgNPs to the chitosan-based MIP sensors, even if positive sometimes, is not overally positive and therefore it is not going to be study the use of them in the other organic acid sensors.

5.5. AgNPs/Chitosan-based MIP sensors comparison

Two different AgNPs/chitosan-based MIP sensors were prepared and shown in previous sections, being one of those sensors prepared for the detection of catechol, as a representative of phenols, and the other one prepared for the detection of tartaric acid.

The purpose of this brief section is to show the different responses obtained for the prepared sensors, and how they obtain specific signal in the study of their corresponding solutions analyse via cyclic voltammetry. Figure 45 shows the analysis of a 10^{-3}M catechol solution (black), it can clearly be seen the characteristic redox peaks mentioned previously for catechol. Figure 45 also shows the response obtained for the analysis of a 10^{-3}M tartaric acid solution (blue), showing the characteristic peaks as well mentioned before, the silver oxidation peak and the O_2 reduction. The signals obtained for the analysis of each solution using the corresponding prepared sensor are easily differentiated and demonstrate the specific responses of the prepared AgNPs/CS sensors.

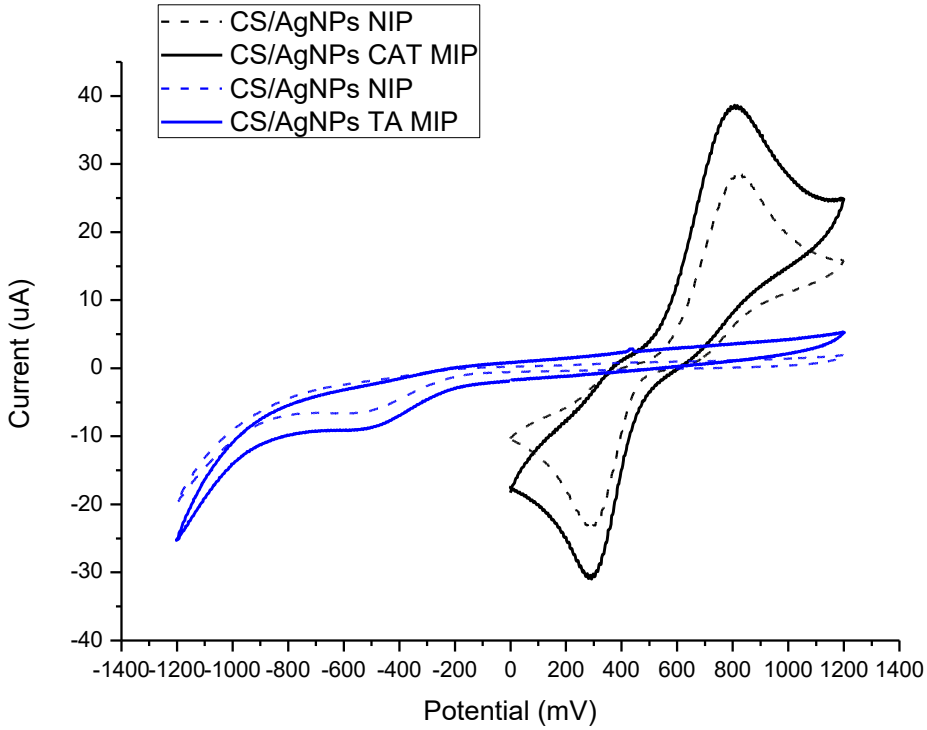

Figure 45. Cyclic voltammogram response of: a CS/AgNPs CAT MIP vs a 10^{-3}M catechol solution (black); a CS/AgNPs TA MIP vs a 10^{-3}M tartaric acid solution (blue).

Conclusions

The results obtained and studied during the present work, lead to the obtention of four major conclusions, which are the following:

- A method was successfully developed to prepare chitosan-based MIP sensors using glassy carbon electrodes, for the detection of compounds of interest in the food industry.

- The preparation of chitosan-based MIP sensors for the detection of catechol, lactic acid, malic acid and tartaric acid was successful and capable of obtaining limits of detection in the order of 10^{-5}M or lower.

- The cross selectivity was evaluated and proved the specificity of the prepared MIP sensors.

- The addition of metallic nanoparticles, gold and silver, was tested and gave slightly better results than those obtained in absence of nanoparticles. However, their use was discarded due to their higher cost of operation which is not compensated by the upgrade of the results, since those are similar to the ones obtained without metallic nanoparticles.

Experimental section

7.1. Materials and methods

Silver nitrate ($AgNO_3$), gold chloride trihydrate ($HAuCl_4 \cdot 3\ H_2O$), sodium borohydride ($NaBH_4$), sodium citrate, chitosan (medium molecular weight), catechol, lactic acid, malic acid and tartaric acid were purchased from Sigma-Aldrich (Saint Louis, MO, USA). Phosphate buffered saline (PBS; pH 7.4, 0.1 M) was prepared with Na_2HPO_4, NaH_2PO_4 and NaCl salt also obtained from Sigma Aldrich (Darmstadt, Germany). Glutaraldehyde (50% aqueous solution) was purchased from Alfa Aesar (Haverhill, MA, USA). Potassium chloride (KCl) and glacial acetic acid were provided by PanReac AppliChem (Barcelona, Spain). Sodium hydroxide (NaOH) was provided by Probus.

Aqueous solutions were prepared using Milli Q water (resistivity 18.2 MΩ·cm) (Millipore-Sigma Aldrich, Darmstadt, Germany). Glassy-carbon voltammetry electrodes (3.0mm diameter) were provided by Sigma-Aldrich.

Electrochemical measurements were performed by cyclic voltammetry at room temperature using a PGSTAT128 potentiostat/galvanostat (AutolabMetrohm, Utrecht, The Netherlands) connected to Nova software. The 50 mL electrochemical cell was based on a three electrode system: a platinum plate as an auxiliary electrode, an Ag/AgCl reference electrode and a glassy-carbon electrode (GC) as the working electrode. All potentials are reported versus the Ag/AgCl reference electrode. pH adjustments were made using a Crison micropH 2000 pH meter. After measurements the glassy carbon electrodes were cleaned by polishing using MicroCut® Silicon Carbide grinding papers provided by Buehler and rinsed with water.

UV–Vis characterization of AuNPs and AgNPs was performed using a UV-2600 device (Shimadzu., Duisburg, Germany).

Standard solutions employed to analyse the response of the sensor were prepared using different quantities of template molecules (to obtain multiple concentrations) and dissolving them in 0.1M KCl, previously prepared using Milli Q water.

7.2. Preparation of Chitosan-based MIP sensors

The preparation of the chitosan-based MIP sensor was based on the electrodeposition of a chitosan solution in a glassy carbon electrode.

Firstly, a 1.5 mg/mL chitosan acid solution is prepared; to do so chitosan is dissolved in acetic acid (30%) and 0.1M PBS (70%). After that a 0.1M solution of the template molecule, except for the case of lactic acid (which is 10^{-4}M), is prepared using the 1.5

mg/mL chitosan solution. The pH of the solution, which initially is around 2.3, can be modified adding NaOH.

The electrodeposition of the chitosan solution containing the template molecule is performed using cyclic voltammetry applying a bias voltage from -1.5V to 0.5V for 10 scans at a scan rate of 0.1 V/s. [33]

After the electrodeposition the electrode is exposed to glutaraldehyde (25% volume) vapours for 20 minutes. The template molecule was eluted in 0.1 M KCl solution under stirring during 20 minutes.

The molecular non-imprinted polymer (NIP) was prepared under the same conditions but in the absence of the template molecule.

7.3. Preparation of Chitosan-based MIP sensors with Gold Nanoparticles

The preparation of chitosan-based MIP sensors with Gold Nanoparticles (AuNPs) needed first the synthesis of the aqueous gold nanoparticles. Turkevitch et al.'s[71] method modified by Frens[72] was used to prepare spherical nanoparticles in aqueous solution.

For the synthesis of gold nanoparticles (Au NPs), the cleanliness of the material is of particular relevance. The material is cleaned with aqua regia (1:3 HNO_3:HCl) and dried. The synthesis started with the addition of 25 mL of a 0.25 mM solution of trihydrate tetrachloroauric acid in an Erlenmeyer flask with a stirrer inside. Subsequently, stirring was activated at 150 rpm and the thermal resistance of the plate was set to 150 °C.

When the solution began to boil, a volume of 180 µL of a 17mM sodium citrate solution was added drop by drop. Upon completion of the addition, the reaction mixture was allowed to stir for 20 minutes at 100 ºC, adding Milli-Q deionized water drop by drop to maintain a constant volume. The solution colour changes from colourless to reddish.

Once prepared the AuNPs solution is mixed with the chitosan solution in a 1:2 AuNPs:CS volume ratio. The chitosan solution presents the corresponding, 0.1 or 10^{-4}M, concentration of template molecule.

The preparation of the MIP sensor was carried out under the same conditions described in the 6.2. section but employing the 1:2 AuNPs:CS solution.

7.4. Preparation of Chitosan-based MIP sensors with Silver Nanoparticles

The preparation of chitosan-based MIP sensors with Silver Nanoparticles (AgNPs) needed first the synthesis of the aqueous silver nanoparticles.[73]

30 mL of a 2mM solution of $NaBH_4$ is added to an Erlenmeyer flask and stirred until the temperature is uniform (at about 400 rpm). Then 10 mL of a 1mM solution of $AgNO_3$ is added drop by drop using a glass pipette, the addition should take around 3 minutes, and

it can be seen the change of the solution colour from colourless to yellowish. The AgNPs solution has to be kept in the fridge and away of light to avoid oxidation.

Once prepared the AgNPs solution is mixed with the chitosan solution in a 1:2 AgNPs:CS volume ratio. The chitosan solution presents the corresponding, 0.1 or 10^{-4}M, concentration of template molecule.

The preparation of the MIP sensor was carried out under the same conditions described in the 6.2. section but employing the 1:2 AgNPs:CS solution.

Bibliography

[1] P.-L. Viollet, *Comptes Rendus. Mécanique* **2017**, *345*, 570-580.

[2] L. D. Claxton, *Mutat Res Rev Mutat Res* **2015**, *763*, 30-85.

[3] M. Xu, J. M. David and S. H. Kim, *International Journal of Financial Research* **2018**, *9*.

[4] H. Lasi, P. Fettke, H.-G. Kemper, T. Feld and M. Hoffmann, *Business & Information Systems Engineering* **2014**, *6*, 239-242.

[5] J. O. Effoduh, *The Transnational Human Rights Review* **2016**, *3*.

[6] G. Tsaramirsis, A. Kantaros, I. Al-Darraji, D. Piromalis, C. Apostolopoulos, A. Pavlopoulou, M. Alrammal, Z. Ismail, S. M. Buhari, M. Stojmenovic, H. Tamimi, P. Randhawa, A. Patel, F. Q. Khan and R. Abbassi, *Journal of Sensors* **2022**, *2022*, 1-18.

[7] S. Malik, K. Muhammad and Y. Waheed, *Molecules* **2023**, *28*.

[8] M. Javaid, A. Haleem, R. P. Singh, R. Suman and E. S. Gonzalez, *Sustainable Operations and Computers* **2022**, *3*, 203-217.

[9] A. J. Christy, A. Umamakeswari, L. Priyatharsini and A. Neyaa, *Journal of King Saud University - Computer and Information Sciences* **2021**, *33*, 1251-1257.

[10] Rinat Galin and Roman Meshcheryakov 2019 *IOP Conf. Ser.: Mater. Sci. Eng.* **537** 032073

[11] D. L. M. Nascimento, V. Alencastro, O. L. G. Quelhas, R. G. G. Caiado, J. A. Garza-Reyes, L. Rocha-Lona and G. Tortorella, *Journal of Manufacturing Technology Management* **2019**, *30*, 607-627.

[12] D. Akinwande, C. Huyghebaert, C.-H. Wang, M. I. Serna, S. Goossens, L.-J. Li, H. S. P. Wong and F. H. L. Koppens, *Nature* **2019**, *573*, 507-518.

[13] Mansoori, G.; Fauzi Soelaiman, T., *J. ASTM Int.* **2005**, 2, 1–22.

[14] R.P. Feynman, There's plenty of room at the bottom. *Eng. Sci.* **1960**, 23, 22–36.

[15] Taniguchi, N.; Arakawa, C.; Kobayashi, T. On the basic concept of nano-technology. In Proceedings of the International Conference on Production Engineering, Tokyo, Japan, 26–29 August 1974.

[16] P. Iqbal, J.A. Preece and P.M. Mendes, *Supramolecular Chemistry* **2012**.

[17] S. Bayda, M. Adeel, T. Tuccinardi, M. Cordani and F. Rizzolio, *Molecules* **2019**, *25*.

[18] S. Prajapati, B. Padhan, B. Amulyasai and A. Sarkar in *Nanotechnology-based sensors*, **2020**, pp. 237-262.

[19] Göpel, W. *et al.* (1991) *Sensors: A comprehensive survey. 2 Chemical and Biochemical sensors*. Weinheim: VCH.

[20] Y. G. Vlasov, Y. E. Ermolenko, A. V. Legin, A. M. Rudnitskaya and V. V. Kolodnikov, *Journal of Analytical Chemistry* **2010**, *65*, 880-898.

[21] A. Hulanicki, S. Geab and F. Ingman, *Pure & Appl. Chem.* **1991**, *63*,1247-1250.

[22] A. Sinha, Dhanjai, R. Jain, H. Zhao, P. Karolia and N. Jadon, *Mikrochim Acta* **2018**, *185*, 89.

[23] Monk, P.M.S. (2001) *Fundamentals of electroanalytical chemistry*. Wiley.

[24] Scholz, F. (2010) *Electroanalytical Methods Guide to experiments and applications*. Berlin, Heidelberg: Springer Berlin Heidelberg.

[25] M. L. Rodríguez-Méndez, C. Apetrei and J. A. de Saja, *Electrochimica Acta* **2008**, *53*, 5867-5872.

[26] V. Parra, Á. A. Arrieta, J.-A. Fernández-Escudero, M. L. Rodríguez-Méndez and J. A. De Saja, *Sensors and Actuators B: Chemical* **2006**, *118*, 448-453.

[27] G. Li, X. Qi, G. Zhang, S. Wang, K. Li, J. Wu, X. Wan, Y. Liu and Q. Li, *Microchemical Journal* **2022**, *179*.

[28] M. A. Chamjangali, H. Kouhestani, F. Masdarolomoor and H. Daneshinejad, *Sensors and Actuators B: Chemical* **2015**, *216*, 384-393.

[29] V. Singh and S. Krishnan, *Anal Chem* **2015**, *87*, 2648-2654.

[30] M. M. P. S. Neves, M. B. González-García, A. Santos-Silva and A. Costa-García, *Sensors and Actuators B: Chemical* **2012**, *163*, 253-259.

[31] J. J. BelBruno, *Chem Rev* **2019**, *119*, 94-119.

[32] Stefan, R.-I., Staden, J.F. van and Aboul-Enein, H.Y. (2001) *Electrochemical sensors in Bioanalysis*. New York: Marcel Dekker.

[33] F. Zouaoui, S. Bourouina-Bacha, M. Bourouina, N. Jaffrezic-Renault, N. Zine and A. Errachid, *TrAC Trends in Analytical Chemistry* **2020**, *130*.

[34] I. Younes and M. Rinaudo, *Mar Drugs* **2015**, *13*, 1133-1174.

[35] Y. Wang, E. Wang, Z. Wu, H. Li, Z. Zhu, X. Zhu and Y. Dong, *Carbohydr Polym* **2014**, *101*, 517-523.

[36] I. Hamed, F. Özogul and J. M. Regenstein, *Trends in Food Science & Technology* **2016**, *48*, 40-50.

[37] K. Gupta and F. Jabrail, *Carbohydrate Polymers* **2006**, *66*, 43-54.

[38] C. Salvo-Comino, I. Rassas, S. Minot, F. Bessueille, M. Arab, V. Chevallier, M. L. Rodriguez-Mendez, A. Errachid and N. Jaffrezic-Renault, *Materials (Basel)* **2020**, *13*.

[39] S. Wu, K. Li, X. Dai, Z. Zhang, F. Ding and S. Li, *Microchemical Journal* **2020**, *155*.

[40] C. Zhao, G. P. Jin, L. L. Chen, Y. Li and B. Yu, *Food Chem* **2011**, *129*, 595-600.

[41] B. Liu, H. T. Lian, J. F. Yin and X. Y. Sun, *Electrochimica Acta* **2012**, *75*, 108-114.

[42] L. Lin, H.-T. Lian, X.-Y. Sun, Y.-M. Yu and B. Liu, *Analytical Methods* **2015**, *7*, 1387-1394.

[43] H.-T. Lian, B. Liu, Y.-P. Chen and X.-Y. Sun, *Analytical Biochemistry* **2012**, *426*, 40-46.

[44] F. Zouaoui, S. Bourouina-Bacha, M. Bourouina, I. Abroa-Nemeir, H. Ben Halima, J. Gallardo-Gonzalez, N. El Alami El Hassani, A. Alcacer, J. Bausells, N. Jaffrezic-Renault, N. Zine and A. Errachid, *Sensors and Actuators B: Chemical* **2020**, *309*.

[45] C. Zhao, G. P. Jin, L. L. Chen, Y. Li and B. Yu, *Food Chem* **2011**, *129*, 595-600.

[46] Y. Wu, X. Feng, S. Zhou, H. Shi, H. Wu, S. Zhao and W. Song, *Microchimica Acta* **2013**, *180*, 1325-1332.

[47] P. Deng, Z. Xu, J. Li and Y. Kuang, *Microchimica Acta* **2013**, *180*, 861-869.

[48] S. Li, D. Du, J. Huang, H. Tu, Y. Yang and A. Zhang, *The Analyst* **2013**, *138*.

[49] T. Kuda, D. Kyoi, H. Takahashi, K. Obama and B. Kimura, *Mar Pollut Bull* **2011**, *62*, 1622-1627.

[50] L. Huang, Y. Lu, Z. Wu, M. Li, S. Xiang, X. Ma and Z. Zhang, *Environments* **2017**, *4*.

[51] L. Sochorova, L. Torokova, M. Baron and J. Sochor, *International Journal of Electrochemical Science* **2018**, *13*, 9145-9165.

[52] F. A. Castillo Martinez, E. M. Balciunas, J. M. Salgado, J. M. Domínguez González, A. Converti and R. P. d. S. Oliveira, *Trends in Food Science & Technology* **2013**, *30*, 70-83.

[53] C. Marques, A. R. Sotiles, F. O. Farias, G. Oliveira, M. L. Mitterer-Daltoé and M. L. Masson, *Arabian Journal of Chemistry* **2020**, *13*, 9118-9129.

[54] https://www.un.org/sustainabledevelopment/

[55] T. Kasa and T. Solomon, *American Journal of Physical Chemistry* **2016**, *5*.

[56] C. Fernandez-Blanco, M. Mugica, M. A. Rodriguez-Perez, C. Garcia-Cabezón and M. L. Rodriguez-Mendez, *Journal of Sensors* **2018**, *2018*, 1-9.

[57] C. Salvo-Comino, A. Gonzalez-Gil, J. Rodriguez-Valentin, C. Garcia-Hernandez, F. Martin-Pedrosa, C. Garcia-Cabezon and M. L. Rodriguez-Mendez, *Sensors (Basel)* **2020**, *20*.

[58] C. Salvo-Comino, I. Rassas, S. Minot, F. Bessueille, M. Arab, V. Chevallier, M. L. Rodriguez-Mendez, A. Errachid and N. Jaffrezic-Renault, *Materials (Basel)* **2020**, *13*.

[59] C. Salvo-Comino, I. Rassas, S. Minot, F. Bessueille, M. L. Rodriguez-Mendez, A. Errachid and N. Jaffrezic-Renault, *Mater Sci Eng C Mater Biol Appl* **2020**, *110*, 110667.

[60] J. Lurie, *Handbook of Analytical Chemistry*, Moscow: Mir, **1978**.

[61] L. Kaewsichan, S. Chooklin and J. Kaewsrichan, *Electronic Journal of Biotechnology* **2011**, *14*.

[62] T. C. Pereira and N. R. Stradiotto, *Mikrochim Acta* **2019**, *186,* 764.

[63] W. J. Bowyer, J. Xie and R. C. Engstrom, *Analytical Chemistry* **1996**, *68* (13), 2005-2009.

[64] M. F. Li, L. W. Liao, D. F. Yuan, D. Mei and Y.-X. Chen, *Electrochimica Acta* **2013**, *110*, 780-789.

[65] A. Robles, M. Fabjanowicz, T. Chmiel and J. Płotka-Wasylka, *TrAC Trends in Analytical Chemistry* **2019**, *120*.

[66] J.-M. Kassaian in *Tartaric Acid*.

[67] G. T. Blair and J. J. DeFraties in *Hydroxy Dicarboxylic Acids*.
[68]A.A. Isse, S. Gottardello, C. Maccato and A. Gennaro, *Electrochemistry Communications* **2006**, *8*, 1707-1712.

[69] A. Ahmad, Y. Wei, F. Syed, M. Imran, Z. U. H. Khan, K. Tahir, A. U. Khan, M. Raza, Q. Khan and Q. Yuan, *RSC Advances* **2015**, *5*, 99364-99377.

[70] H. S. Toh, C. Batchelor-McAuley, K. Tschulik, M. Uhlemann, A. Crossley and R. G. Compton, *Nanoscale* **2013**, *5*, 4884-4893.

[71] J. Turkevich, P.C. Stevenson and J. Hillier, *Discuss. Faraday Soc*. **1951**, *11*, 55–75.
[72] F.M.A. Carpay and W.A. Cense, *Nat. Phys. Sci.* **1973**, *241*, 20–22.
[73] J.A. Creighton, C.G. Blatchford and M.G. Albrecht, *J Chem Soc. Faraday Trans II* **1979**, *75*,790-8.